USING MACHINE LEARNING TO PREDICT SAG AND LEVELING

BEHAVIOR OF INTERIOR ARCHITECTURAL PAINTS

A Thesis

presented to

the Faculty of California Polytechnic State University,

San Luis Obispo

In Partial Fulfillment

of the Requirements for the Degree

Master of Science in Polymers and Coatings Science

by

Ethan Kim

September 2020

COMMITTEE MEMBERSHIP

TITLE: Using Machine Learning to Predict Sag and Leveling Behavior of Interior Architectural Paints

AUTHOR: Ethan Kim

DATE SUBMITTED: September 2020

COMMITTEE CHAIR: Erik Sapper, Ph.D.
Assistant Professor of Chemistry and Biochemistry

COMMITTEE MEMBER: Raymond Fernando, Ph.D.
Professor of Chemistry and Biochemistry

COMMITTEE MEMBER: Shanju Zhang, Ph.D.
Associate Professor of Chemistry and Biochemistry

ABSTRACT

Using Machine Learning to Predict Sag and Leveling Behavior of Interior
Architectural Paints

Ethan Kim

In the world of interior architectural paints, rheology, or the deformation and flow of
a fluid, is one of the largest economic and development hurdles for paint formulators.
To achieve maximum functionality, coverage, and economy of product, the rheology
of the coating must be properly optimized, balancing performance while minimizing
undesirable flow defects such as paint sagging or visible brush and roller marks; these
visual imperfections are associated with the sag and leveling properties of the paint.
Many researchers have attempted to develop a better understanding of sag and lev-
eling, either by drawing correlations or through mathematical derivation; however,
neither approach adequately predicts sag and leveling behavior. This provides the
opportunity for machine learning to create a powerful model that utilizes formulation
and rheological data and industry-standard tests to predict sag and leveling before
the formulator creates the paint, reducing the resources necessary to optimize paint
compared to a heuristic approach. Since little attention has been paid to the full rhe-
ological effects of sag and leveling, this approach also provides a first step in gaining
new insight into the mechanisms behind this behavior.

ACKNOWLEDGMENTS

TABLE OF CONTENTS

LIST OF TABLES

LIST OF FIGURES

Chapter 1

INTRODUCTION

1.1 Introduction to Sag and Leveling of Paints

Interior architectural paints, like all protective or decorative coatings, must be optimized for performance. Ideally, these coatings will form a cohesive, uniform film that provides optimal aesthetics, function, and protection with maximal economy of product, while limiting unsightly defects such as drip or roller marks. These visual imperfections may often be referred to as sag or leveling issues. In general, sag refers to the undesirable flow of a coating down an inclined surface due to gravity; while leveling is the ability of a coating to flow laterally and diminish surface irregularities.[1,2] In real world applications, these imperfections can manifest in many different forms. Brush marks, orange peels, peaks, or craters are tell-tale signs of leveling issues.[2–4] However, sag and leveling are conflicting properties; reducing the paint's resistance to flow or viscosity to provide a more uniform film can cause the paint to drip or sag when applied to a wall.[5,6] Creating a balance between sag and leveling performance is critical in formulating a successful paint, which is further complicated by legislative and market pressures pushing for higher solids paints and less toxic waterborne paints, limiting the amount of solvent and the freedom of choice for the formulator.[7,8]

Traditionally, paints are comprised of three main components: a liquid phase (water and/or solvent), a film-forming latex or polymer solution, and pigments. Additionally, paints may contain a number of process- and performance-enhancing additives like defoamers, rheological modifiers, and biocides.[1] These components and additives can significantly affect how the paint will flow or how it will dry, which can further complicate the sag and leveling process. As solvent or water evaporates, the

1

increased solid content of the film increases the viscosity. Evaporation also causes the system to cool and capillary and osmotic forces act upon the paint itself, forcing latex or polymer particles to pack closer together.[8] As these particles pack closer together and coalesce to form a film, the amount of solvent exposed to the environment decreases, changing the rate of evaporation. Fluid viscosity changes occur as more solvent or water leaves the system, limiting flow as the paint dries.[8,9] Surface tension gradients arise from uneven drying rates, temperature differences, or the diffusion of components such as surfactants, creating tangential shearing forces along the free liquid interface that could overcome yield stress and initiate flow.[3,8,10] The Marangoni flows that arise from these surface tension gradients attempt to minimize the surface energy of the free interface. Flow of the liquid phase from low to high areas of surface energy on the film can increase the local height of the paint film during early stages of evaporation. The reduction in evaporative flux resulting from the increased height allows for more time for gravity to act on the film, increasing sag.[9] Marangoni flows may also assist in leveling; however, localized low surface energies from contaminants or surfactants that occur as the paint dries lead to crater formation as the liquid phase is driven away.[4,11] Defects may also form if the surface tension is uniform. Irregular substrate geometry could cause local variations in film curvature and along with surface tension, cause capillary pressure gradients that drive the coating to become non-uniform in thickness. This non-uniformity will produce high stresses aggravated by gravitational flow and decrease the local viscosity, increasing flow.[7] Furthermore, environmental conditions must be considered. The ambient temperature can significantly affect the drying rate and cause surface tension gradients. Higher temperatures also provide more thermal energy, requiring less energy input to initiate flow.[12] Humidity can decrease the rate of evaporation, allowing for more time for sag to affect the coating.

Furthermore, the viscosity of the paint will change during and after application. When applied by brush, paint will undergo shear forces as illustrated in Figure 1.1 below. A shear force F is applied coplanar to the top layer, deforming the paint film denoted in blue and inducing flow while the red reference or substrate layer remains stationary.[13] The resultant shear stress is the applied shear force divided by the area of the plate A. The rate at which this deformation or strain is applied is the shear rate and is the difference in velocity between the top and bottom plate divided by the shear gap h.
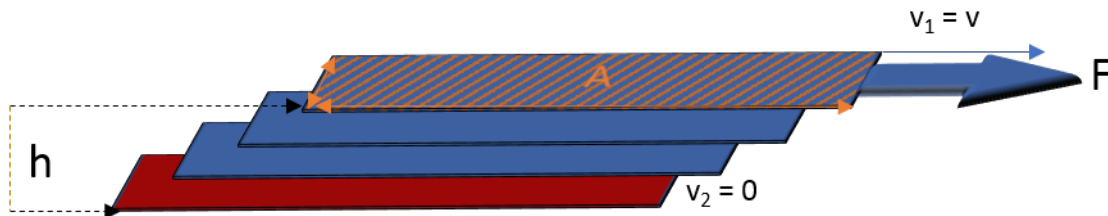
Figure 1.1: Visualization for how shear rates and stresses are calculated.

The viscosity of the fluid is a local material property and thus, will vary as local conditions vary such as temperature, shear rate, and recent shear exposure.[14] As shear rates increase, the structure of the material may break apart and lower the viscosity. Ideally, a paint will readily flow at high shear rates as it is applied to the substrate and when applied, the viscosity must be balanced at lower shear rates associated with gravity and surface tension effects to prevent sagging and levelling issues.[7,15–17]

However, not only does viscosity change as the shear rates change, but viscosity changes within the bulk of the film itself. When applied to a vertical substrate, the shear stresses caused by gravity differ between the substrate-coating interface and the free surface. The difference in viscosity between these two layers could easily be two orders of magnitude or more, meaning a single viscosity calculation is insufficient to accurately reflect the forces involved in sag and leveling.[5,7] The gravitational shear stresses will reach a maximum at the substrate to zero at the free interface.[5]

Despite these complexities, researchers and formulators have utilized a more holistic approach to evaluating sag and leveling. The ASTMs D4400 for sag and D4062 for leveling apply pre-sheared paint on black and white Leneta charts.[2,18] A notched applicator is used to evaluate sag, with each successive notch corresponding to an increasing notch clearance height. Different anti-sag meter applicators are utilized for specific coating types: solvent-borne architectural, industrial O.E.M. coatings, high build coatings, and water borne architectural. The anti-sag meter is drawn down over the paint in a straight line, then immediately hung on its side, with the thinnest stripe at the top. The sag chart is left to dry and evaluated to determine the degree to which the preceding stripe (post-index stripe) has bled into the lowest stripe that has resisted sagging (index stripe). The degree to which post-index stripe merged with the index stripe corresponds to an addendum fraction. This fraction is multiplied by the difference between the index and post-index stripe number, then added to the index stripe number to obtain the anti-sag index.[18] The leveling test utilizes a grooved cylindrical rod with ridges 0.3 mm deep and 1.25 mm wide to draw down over the applied coating in a straight line. The leveling chart is left on a flat surface to dry and evaluated against a levelness standard, where it will be given a numerical rating between 0 (very poor leveling) and 10 (perfect leveling or no perceptible ridges).[2] While established as a useful qualitative assessment of paint performance, these ASTMs can become a source of misery for researchers attempting to characterize or control sag and leveling behavior. These ASTMs evaluate endpoint sag and leveling behavior without taking into consideration rheological or flow behavior or paint drying effects. Therefore, a new method for analyzing sag and leveling that utilizes flow behavior in its analysis is necessary.

1.2 Sag and Leveling and Rheological Characterization

A more robust understanding of rheology, the study of the flow and deformation of materials, is necessary to characterize or control sag and leveling behavior. In industry practice, it is common to use single point viscosity measurements (Brookfield, KU, ICI) to rheologically characterize the paint at low (0.1-10 s^{-1}), mid (100 s^{-1}) and high shear (10,000 s^{-1}) conditions. However, sag and leveling behavior is not dependent on single point measurements and as the paint is applied and dried, it is acted upon by a number of forces as well as time. The ideal viscosity for different processes will differ depending on the shear rate, allowing for the paint to flow readily or provide resistance to flow, as seen in Figure 1.2. During brush application, the paint is subject to high shear rates between 1,000 to 10,000 s^{-1}.[17] At these high shear rates, an ideal paint is expected to readily flow for ease of application. However, at low shear rates associated with gravity, the paint should thicken but at a slower rate to achieve sufficient leveling without allowing for any sag.[19] In other words, the ideal paint's viscosity is dependent on the applied shear rate. Furthermore, when a shear rate is applied to a paint, the resultant stress may not be achieved instantaneously due to the particles and/or molecules rearranging in the direction of flow or the structure of the system may change, such as the breaking of weak bonds or aggregation of particles. This may cause a decrease in viscosity. Once the shear is removed, the structure begins to reform and rearrange, increasing viscosity over time. This time-dependent change in viscosity is known as thixotropy.[13] Because paint should thicken slowly to provide sufficient leveling while limiting sag after shear, thixotropy should play a key role in sag and leveling behavior.
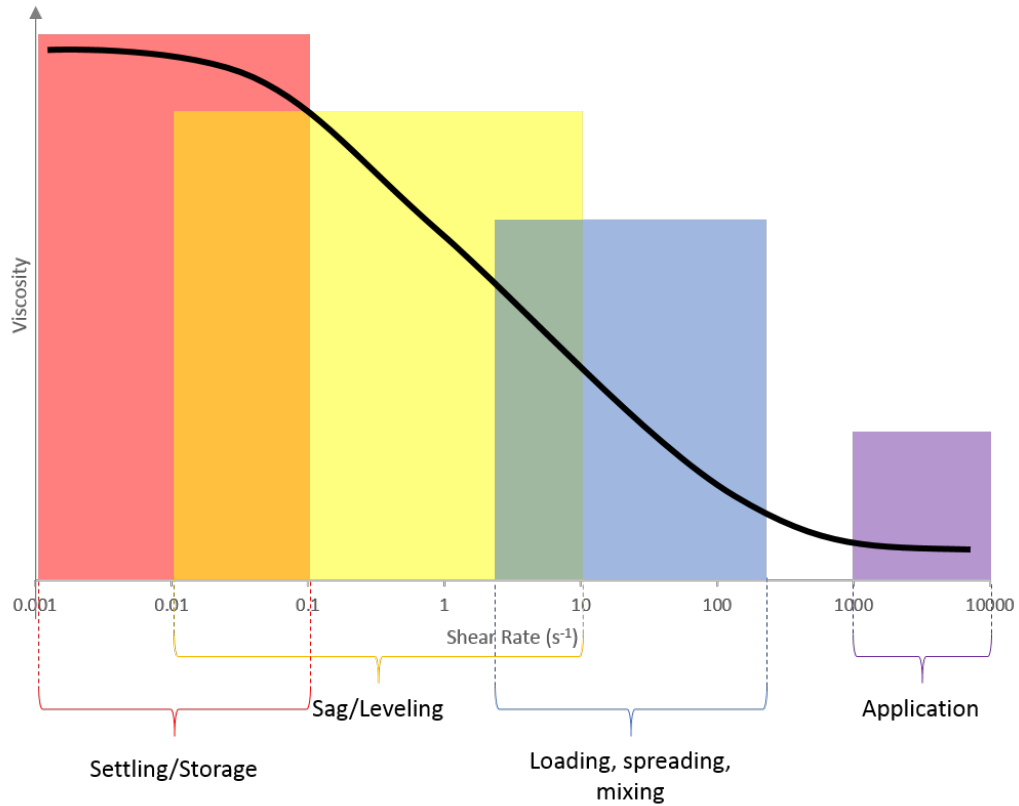
Figure 1.2: Shear rates associated with sag and leveling and other processes.

1.2.1 Rheological Flow Models

Rheological flow behavior can be classified as Newtonian, where the apparent viscosity is independent of applied shear rate, or non-Newtonian, which can encompass a large variety of shear-rate-dependent viscosity profiles. Newtonian behavior is limited only to simple fluids like water or very dilute solutions and can be described by Equation 1.1 below:

$$Stress(\sigma) = Viscosity(\eta) \cdot ShearRate(\dot{\gamma}) \tag{1.1}$$

Non-Newtonian fluids can be described over a limited range of shear rates by a basic power law function and divided into pseudoplastic or shear-thinning ($n < 1$) and

dilatant or shear-thickening ($n > 1$) materials, as shown by Equation 1.2 below:[8]

$$\sigma = K\dot{\gamma}^n \tag{1.2}$$

Shear-thinning fluids like paint decrease in apparent viscosity as the shear rate increases. Shear-thickening fluids increase in apparent viscosity in response to an increase in shear rate. The power law function fits experimental results over two or three decades of shear rate; however, at high shear rates, the power law function fails as the viscosity is increasingly predicted to reach a finite value. Other models such as the Sisko model rectify this issue by including the high-shear Newtonian region.[13] Some fluids contain a characteristic yield stress or a minimum stress necessary to overcome initiate flow or some irreversible deformation.[7] This is considered ideal for paints, as the yield stress will counter defects such as sag, dripping, crater formation during application and film formation and provide in-can stability by preventing flocculation and sedimentation of pigment particles during storage. However, yield stress can cause leveling to cease if the surface tension stress falls below the yield stress and by affecting the low shear viscosity through remnants of structure responsible for yield behavior.[5] An ideal yield stress is where the material acts like an ideal Hookean (elastic) solid before yielding and becoming a viscous fluid. An ideal Hookean solid is defined in Equation 1.3 below where the stress is proportional to the deformation or strain by the strain modulus G'.

$$\sigma = G'\gamma \tag{1.3}$$

Inclusion of a yield stress factor modifies a linear model with an added yield stress (Bingham), a square root of the Bingham model (Casson), and a power law function with an added yield stress variable (Herschel-Bulkley) as seen in Equations 1.4, 1.5,

and 1.6 below.[20]

$$\sigma = \sigma_y + \eta_p \dot{\gamma} \tag{1.4}$$

The Bingham equation (1.4) describes the stress/shear rate behavior of many shear thinning materials at low shear rates; however, the value of the yield stress is dependent on the range of shear rates the yield stress is extrapolated from. The viscosity is referred to as plastic viscosity when the fluid is described by Bingham flows.[21]

$$\sigma^{\frac{1}{2}} = \sigma_0^{\frac{1}{2}} + \eta^{\frac{1}{2}} \dot{\gamma}^{\frac{1}{2}} \tag{1.5}$$

Plotting the Casson (1.5) provides a straight line to determine σ_0 and η; however, this linear relationship will only hold true above certain shear rates.

$$\sigma = \sigma_y + K\dot{\gamma}^n \tag{1.6}$$

As the most widely used model, the Herschel-Bulkley model (1.6) fits most architectural paint curves. When $\sigma = 0$, the function is reduced to the power law equation. When $n = 1$, the function becomes the Bingham model. When $\sigma = 0$ and $n = 1$, the function describes Newtonian behavior.

The Cross Equation is used for curves that have limiting viscosities at the low (η_0) and high(η_∞) shear ends. These two regimes are separated by a shear thinning region and is described by Equation 1.7 below with time constant K, sometimes referred to as the consistency, and dimensionless constant m.[13,22]

$$\frac{\eta - \eta_\infty}{\eta_0 - \eta_\infty} = \frac{1}{1 + K\dot{\gamma}^m} \tag{1.7}$$

Cross found that adjusting m to 2/3 allowed for application to published data on polymer dispersions, polymer systems, and molten polymers and a value of 1 could be applied to monodisperse linear polymers.[23]

A variant of the Cross equation is given by Carreau in Equation 1.8 below:

$$\frac{\eta - \eta_\infty}{\eta_0 - \eta_\infty} = \frac{1}{\left(1 + (K\dot{\gamma})^2\right)^{\frac{m}{2}}} \tag{1.8}$$

Reducing the Carreau equation when $\eta << \eta_0$ and $\eta >> \eta_\infty$ yields the power law model. When $\eta << \eta_0$, the Sisko model can be derived as seen in Equation 1.9 below.[13,22]

$$\eta = \eta_0 + K\gamma^n \tag{1.9}$$

The Sisko model can be useful in describing flow in the power law and high shear Newtonian regions.[22]

These models are fit to a flow curve in a flow sweep experiment run typically in a controlled shear rate rheometer. In a flow sweep experiment, a constant shear rate is applied to a sample and a viscosity measurement is taken when the sample has reached steady state flow when the stress or strain is constant. The shear rate is increased, and the measurement process is repeated. The flow sweep provides a graph with point viscosity measurements and the associated stress and strain rate ($\dot{\gamma}$).[9,14] Measurement can also be done with a controlled stress rheometer, where a constant stress is applied until the shear rate becomes constant.[5]

Caution should be taken when utilizing these flow models; extrapolating to measure yield stress at a zero shear rate can yield inconsistent results. Since these models cannot encompass the complexities of the paint curve shapes, the models can only fit limited regions of the curve. This means that the calculated yield stress may vary depending on which region of the curve is utilized, making model-fitting a labor in-

tensive, iterative process that gives varied results.[5] The yield stress calculated from the extrapolation of a flow curve could provide a yield stress much lower than those gathered from other experiments.[12,24,25] Because the yield stress is determined under shear rather than from starting at rest, the difference in yield stress values could be attributed to the thixotropic behavior of the material as well as the structure remaining present in less destructive techniques. Furthermore, when applying a shear rate to the material, it has already "yielded", therefore it is impossible to obtain a direct measurement of yield stress, thus requiring model extrapolation.[5] The yield stress calculated from flow curves will sometimes be referred to as "dynamic yield stress" whereas yield stress determined from experiments starting at rest will be referred to as "static yield stress".[12,24] Dynamic yield stress can be useful in determining the effect of yield behavior on leveling following structural breakdown, while static yield stress is useful for sedimentation or flocculation studies.[5] Furthermore, Dinkgreve *et al.* found significant disagreement among yield stress values for a commercial hair gel and non-thixotropic model dispersions, depending on the method of measurement used.[25]

There has also been much discussion on whether there exists such "true" yield behavior where the material first acts like an ideal Hookean elastic solid before suddenly yielding and becoming a viscous fluid, first challenged by Barnes and Walters in 1985.[26,27] However, there is the existence of "apparent" or "observable" yield behavior in which the viscosity drops precipitously under small stresses. For example, a 6% by volume suspension of iron oxide in mineral oil showed a 105-fold drop in viscosity from 0.7 Pa to 3 Pa.[28] Furthermore, time dependency is also relevant when discussing yield stress; when considering sedimentation or flocculation resistance in paint, the time scale for stress to act on the system is much longer than for sag or leveling considerations. Therefore "true" yield behavior is much more significant for sedimentation or flocculation applications.[5]

There are other issues as well with utilizing flow curves to evaluate the rheology of paints. The prevalence of controlled shear rate rheometers in industry practices have led to shear rate being treated as the independent variable. This has become the prevailing methodology for decades and has recently been challenged by Richard Eley in both their 2005 review and 2019 review of paint rheology.[5,7] Eley argues that shear rates are not independent of rheology and is dependent on and determined by the interaction between the viscosity of the material and the shear stress. Because shear rates will vary with the viscosity of the paint under the same shear stress, the gravitational stresses that drive sag will show lower shear rates (a measure of coating flow) with higher viscosities of paint. The diagram of coating flow processes at characteristic shear rates should instead have a slanted trapezoid to the left, rather than a rectangular bar. This is visualized in Figure 1.3 below.
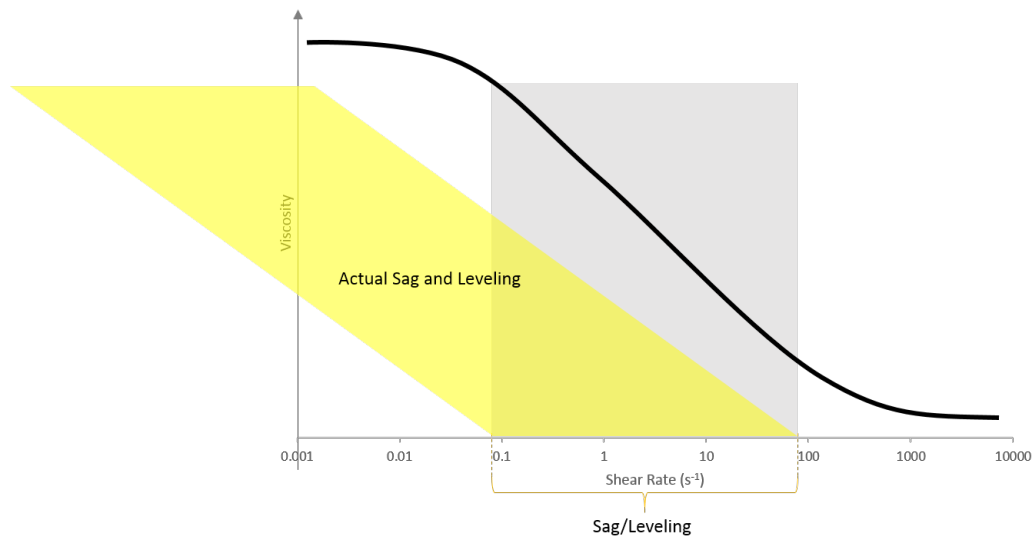
Figure 1.3: Eley's proposed view of coating film processes at shear rates.

Shear stress, Eley argues, should be the controlling variable in coating flows. Rearranging Equation 1.1 yields Equation 1.10 below, where the shear rate is dependent

on the viscosity at the operative shear stress:

$$\dot{\gamma} = \frac{\sigma}{\eta} \tag{1.10}$$

Utilizing shear stresses confers a significant advantage over the current prevailing shear rate mentality: the sum of the forces acting on the coating translate to stress and because the component force-vectors are additive or subtractive, surface tension, gravitational, body, and centrifugal forces can be incorporated within a range of shear stresses, independent of the rheology. Highlighting the problems with the current methodology is the lack of agreement on characteristic shear rates. Quach and Hansen found the initial shear rates to be around 50 to 100 s^{-1}.[29] Khanna estimates the shear rate to be as low as 0.5 s^{-1}.[30] Wu estimates the shear rates associated with sag to be in the range of 0.001 to 0.1 s^{-1}.[31] Dodge estimates the range to be from 0.5 to 0.1 s^{-1}.[32] Kurnam and Raaschou estimates the characteristic shear rates to be from 0.001 to 0.5 s^{-1}.[16] Deka *et al.* state that the leveling shear rate range extends from 0.01 to 1 s^{-1}.[33] Colclough *et al.* showed that for variations in the paint film thickness, viscosity, surface tension, and substrate geometry, the shear rates associated with sag and leveling could easily vary from 0.1 to 100 s^{-1}.[34] However, much of the literature regarding sag and leveling processes still use shear rates as the controlling variable in coating flows. It is possible that the discrepancy found in characteristic shear rates and rheological correlations to sag and leveling can be associated with this mindset, requiring a possible change in practice or utilizing rheological tests other than flow sweeps to investigate correlations to sag and leveling behavior.

1.2.2 Dynamic Oscillatory Tests

Dynamic oscillatory tests have been used to examine the response of the material to an oscillating stress at an angular frequency ω (rad/s). Torque or rotation is applied

to the material for a short time in one direction before reversing and applying the force in the opposite direction for the same amount of time. The process is repeated until a steady response for strain is observed, where it oscillates with the same frequency as the applied stress. The material could respond in a few ways. An ideal elastic response, where the maximum strain amplitude response is in the same position as the maximum stress amplitude, or an ideal viscous response where the response is shifted to maximum energy dissipation. In the case of an ideal viscous response, the strain and stress sine waves are shifted by $\omega t = \pi/2$. This shift in stress and strain is known as the phase angle; likewise, for an ideal elastic response, there is no shift in stress and strain and the phase angle is 0. For a viscoelastic system, the phase angle is between $\pi/2$ or 90° and 0 since it will display both viscous and elastic behavior. The viscoelastic responses are visualized in Figure 1.4 below.
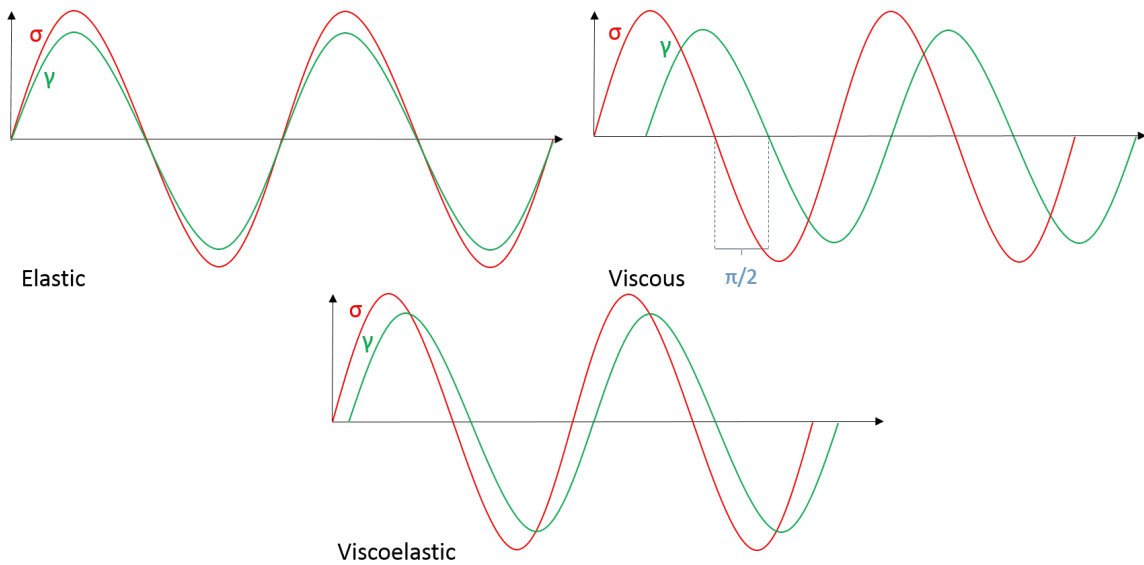
Figure 1.4: Stress-strain responses for an ideal elastic, viscous, and viscoelastic system.

The ratio of the maximum stress to the maximum strain is the complex modulus G^* as seen in Equation 1.11 below.[8,13,35]

$$|G^*| = \frac{\sigma_0}{\eta_0} \qquad (1.11)$$

The complex modulus can be resolved into the storage modulus (G'), a measure of stored energy, and loss modulus (G''), a measure of stress dissipated as heat, through the Fourier transform in Equation 1.12 below:

$$G^* = G' + iG'' \qquad (1.12)$$

The two modulus components can then be written with respect to the phase shift in Equations 1.13 and 1.14 below:

$$Storage\ Modulus\ (G') = G\cos(\delta) \qquad (1.13)$$

$$Loss\ Modulus\ (G'') = G\sin(\delta) \qquad (1.14)$$

The ratio of the loss and storage moduli is known as the loss tangent or $\tan(\delta)$, as seen in Equation 1.15 below:

$$\tan(\delta) = \frac{G''}{G'} \qquad (1.15)$$

The loss tangent indicates the relative degree of energy dissipation. At $\tan(\delta) = 1$, the phase shift is 45°, meaning the material equally demonstrates elastic and viscous character, depending on the frequency or rate of deformation. When $\tan(\delta) > 1$, the viscous behavior dominates. At $\tan(\delta) < 1$, the substance responds to deformation elastically.[5,35,36] At small stresses, the material will display viscoelastic behavior at the linear viscoelastic region, where both moduli remain constant until it reaches a

critical strain. Beyond this critical strain, the material will decrease in viscosity and the microstructure of the material will break down..[14,36]

Frequency sweep tests, where the strain amplitude is kept constant at a value typically within the linear viscoelastic region while the angular frequency ω changes, are best utilized for insight into long term stability. Conversely, oscillatory amplitude sweep tests, where the angular frequency is kept constant and G^*, G', and G'' are measured as a function of strain amplitude, can be utilized to determine the yield stress. In amplitude sweep plots, the critical strain is measured at which the storage modulus G' begins to decrease. Some consider this to be the yield point, as it represents structural breakdown. Alternatively, the crossover point of the G' and G'' moduli could be considered the yield point, where G'' begins to become larger than G'. Beyond this point, $tan(\delta) > 1$ and the viscous behavior will dominate, indicating flow.[5,13,35] Both methods have seen utilization in literature. However, both methods will provide significantly different values of yield stress; Dinkgreve *et al.* found that using the crossover point yielded the highest calculated yield stress, twice that of the Herschel-Bulkley extrapolated value from the flow curve.[25] Fernandes *et al.* suggest that there are two stages involved with the yielding process. The first involves the transition from linear to nonlinear viscoelastic behavior, where the material changes from an ordered state to a disordered state, capable of irreversible deformation or flow. The second stage, where yielding actually occurs, happens at stresses higher than the crossover point because G' and G'' are only correctly defined within the linear viscoelastic region.[24] Eley in their 2019 review believes that the crossover point is the best method for determining yield stress as the crossover method is the method with the least ambiguity. However, in his study of 13 semigloss paints, only five of those paints could have yield stress determined through the crossover method.[5] It should be noted that the frequency at which the test is run will influence the yield stress value gathered as well. Since G' generally decreases with decreasing frequency, lower

frequencies will provide a better insight into material properties at rest; however, low frequencies can greatly increase the time of a test.[12,37]

1.2.3 Other Yield Stress Tests

Other tests to determine yield stress could involve the creep test, where a constant stress is applied to the material and the shear rate is measured, allowing one to measure the static yield stress. If the imposed stress is below the yield stress, the resultant shear rate will remain at zero. At stresses exceeding the yield stress, the material will flow, and a nonzero shear rate will be observed. However, this method is inefficient, as knowledge of the approximate yield stress is necessary beforehand or multiple creep tests must be run, and enough time must be allowed for the material to yield at low stresses which makes it sensitive to structural changes.[12,13,24,25] Fernandes *et al.* found that the creep experiment for a commercial hair gel provided a slightly higher static yield stress value to the Herschel-Bulkley extrapolation of dynamic yield stress from a flow curve.[24]

The final method covered to determine yield stress is the stress ramp experiment, where a constant increasing stress is applied, and the shear rate or strain is monitored. Plotting the viscosity over time will yield a peak in viscosity, corresponding to the yield point, after which the material will begin to flow, and the shear rate will drastically increase. Prior to the peak, the material responds elastically, and the strain rate is near constant.[12,25] However, the highest stress at which the response is still elastic is ambiguous, as it might reflect viscoelasticity, and is dependent on the rate of stress.[25]

1.2.4 Thixotropy

While yield stress is an important rheological property in governing paint flow, other properties and tests are useful in understanding flow behavior. Thixotropy is believed to be ideal for paint applications as the time-dependent thickening behavior will counter sag after application while allowing suitable time for leveling to occur. The two methods for determining thixotropy of a paint are the thixotropic loop, where the shear rate or stress is gradually increased over time and then immediately ramped down to examine structural recovery, and the three-interval thixotropy test (3ITT), where the paint at rest conditions is exposed to a constant low shear rate or stress as reference, subjected to a high shear rate or stress for a short period of time to break the internal structure, then returned to the reference low shear rate or stress over a long period of time to determine the extent of thixotropy.[20] The thixotropic loop could be analyzed by taking the enclosed area between the ramp up and ramp down curves; however, Banfill and Saunders have shown that two suspensions of cement pastes with different thixotropic properties give similar hysteresis loops.[38] Thus, thixotropic loops are more of a qualitative measure of thixotropy in a sample. On the other hand, three different quantitative values could be gathered from the three-interval thixotropy test to measure thixotropy. The first is the "thixotropy value", which is the difference in viscosity of the maximum viscosity after structural regeneration and the minimum viscosity after structural decomposition. The second is the "total thixotropy time" which is the time difference from the end of structural decomposition to the time it takes to reach complete structural regeneration. Lastly, the "relative thixotropy time" is the time required to reach a certain percentage of the reference viscosity after structural decomposition.[20]

1.2.5 Effects of Initial Film Geometry

While most research has been dedicated to using rheological parameters during and after application to correlate with sag and leveling performance, one often over-looked influence is the effect of initial surface geometry of the coating after application.[7] This initial film thickness has massive repercussions on how the film will level. The Orchard Equation describes leveling as the decrease in amplitude of a single sinusoidal striation wavelength over time; this assumes that leveling is dominated by the longest wavelength.[39] The Orchard Equation is shown in Equation 1.16 and visualized in Figure 1.5 below.

$$a = a_0 e^{-\frac{16\pi^4 h^3 \eta t}{3\lambda^4 \eta}} \tag{1.16}$$
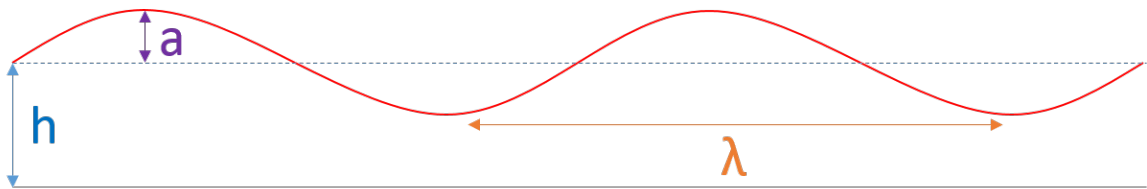
Figure 1.5: The Orchard Equation.

The amplitude decays exponentially over time, dependent on the cube of the average film thickness h and the inverse of the roughness wavelength λ. Increasing the film thickness will substantially increase the rate of leveling; however, too high a film thickness will cause excessive sag and wastes paint. Originally, it was proposed that the peaks and valleys of brushmarks were caused by artifacts of the brush bristle geometry; however, Eley *et al.* found that with the same brush, the brushmark wavelength will vary among paints.[5] Saucy *et al.* also determined from observing brush-applied paint from underneath a glass plate, that brushmarks do not appear to originate from brush bristles; rather, the bristles appear to "float" above the substrate on a liquid "lubrication layer" 1-2 mils thick.[40] Furthermore, application with roller

will also yield striations or ribs. In an early study on brushmarks, Pearson *et al.* found that application by brush, roller, and wedge spreader all resulted in characteristic striations.[41] Pearson also found that striations produced by a wedge spreader could be correlated to a dimensionless variable called the capillary number (Ca), which characterizes the relative effect of viscous and surface tension forces. The capillary number is described in Equation 1.17 below.

$$Ca = \frac{\eta V}{\gamma} \tag{1.17}$$

Where γ is the surface tension, η is the viscosity at the rate of application and V is the velocity of the applicator. For three Newtonian liquids with Ca values between 0.1 and 10, Pearson found that for an increasing capillary number, the frequency of striations increases (or the wavelength of striations decreases).[41] Eley also found that in a set of thirteen semigloss paints, the capillary number ranged from 20 to 230. From this, Eley concluded that viscous forces dominate stabilizing surface tension forces and that brush and roller applications are well above the capillary number for rib formation. Rather than brush bristle geometry dictating the presence of brushmarks, viscous forces instead influence the creation of brushmarks regardless of application method.

Eley has proposed that the formation of brushmarks is likely from a lower stress film-splitting process occurring near the trailing end of the paint brush, as some paint remains attached to the bristles and some is dragged off as the brush is moved. When correlating brushmark frequency as a function of viscosity, Eley found that there was good linear correlation ($R^2 = 0.84$) for shear stress ranges between 50-200 dyn/cm^2 but failed to correlate at shear stresses of 5000 dyn/cm^2, where it would be expected for shear to have an effect on the lubrication layer. Eley also found better leveling correlated to increasing viscosity at shear stresses of 3000 dyn/cm^2, which they associated with increased film thickness during application.[5]

When a film is applied, the layer will be of variable thickness consisting of peaks and valleys. These peaks and valleys are generated from mechanical and hydrodynamic pressure caused through the lubrication layer, which resists brush or roller contact with the substrate, and brush or roller drag, the force resisting brush or roller application. Brush drag may be desirable to ensure adequate transfer and film build. However, the higher the brush drag, the higher the film thickness will be. As a result, the better leveling will be at the potential cost of excessive sag. Excessive brush drag can also make the process of painting overly tiring.[5,17] Chatterjee et al. found that, for HEUR-thickened paints with variable end-hydrophobe lengths, brush drag monotonically increased with the first normal stress difference (N1) at high shear rates. With positive N1 values, the force acts against the direction of paint transfer and thus, the higher the brush drag; likewise, with negative N1 values, the paint assisted application, acting in the direction of paint transfer, thus lowering the brush drag.[17]

While an understanding of rheology is necessary to comprehend the factors that influence sag and leveling, rheological characterization alone does not exactly replicate the application process or environment, making it difficult to relate these conditions with end-use performance.[17] Nevertheless, researchers have attempted to correlate rheological properties to sag and leveling performance with different degrees of success; however, there is little consensus as to what rheological parameter or parameters can correlate to or predict sag and leveling behavior.

1.3 Empirical Correlations to Sag and Leveling

Several researchers have attempted to correlate empirical results to find limits for or predict sag and leveling behavior. As stated before, there is little consensus as to the best predictor for sag and leveling behavior; however, there does appear to be some consensus on the general ranges for rheological behavior. Viscosity at low shear rates

or stresses appear to have an effect on sag or leveling behavior, although the exact shear rate or stress isn't widely agreed upon. Eley in their preference for utilizing shear stresses, finds that viscosity at 10 dyn/cm^2 (1 Pa) or 20 dyn/cm^2 (Pa) seem to correlate well with sag and leveling in their study of 13 semigloss paints.[5] Wu found that viscosity at around 50 poise (5 Pa s) at a shear rate of 1 s^{-1} would provide an adequate balance of sag and leveling.[42] Beeferman and Bergren also define rheological limits for viscosity at "leveling viscosity" should be balanced to prevent sagging while allowing leveling to occur.[43] There is disagreement over the exact shear stress or rate that correlates with sag and/or leveling; however, it is also possible that rather than viscosity at a single shear rate or stress value, a range of shear stresses or rates can parallel sag and leveling forces as well as the changing conditions over time. The general trend observed is that the lower the viscosity at low shear, the better the leveling and the worse the sag and vice versa; therefore, a balance for viscosity at these low shear rates or stresses is necessary for good sag and leveling performance.

Thixotropy as well has been found to have good correlation to sag and leveling behavior, since after high shear exposure, the structure should slowly reform to provide adequate sag resistance without interfering with leveling. Bhavsar and Shreepathi utilized the three interval thixotropy test (3ITT) to utilize the change in viscosity post-high shear to define rheological limits to sag and leveling performance, which will be dependent on the thickener used.[15] Jong, in their study of thickeners, utilized the 3ITT to find that the extent of recovery after high shear leads to better sag resistance, with different thickeners giving different extents of recovery.[44]

Storage and loss moduli and $tan(\delta)$ values have also been correlated to sag and leveling performance. Lu found that the lower the loss modulus at frequencies of 0.01 rad/s, the better the leveling. Due to the lack of correlation of leveling to the storage modulus, Lu concluded that leveling is a viscosity-dominated process.[45] However, the test occurs at a strain far above what most frequency sweeps utilize. While

most frequency sweeps utilize low strains at small frequencies to gain information on colloidal forces between particles, the high strain could be indicative of stresses that relate to leveling or shear. Khanna found that increases in elastic modulus as shear rates increase will lead to better leveling.[30] It should be preferred to have a low elastic shear modulus at low shear rates, where the structure of the paint film does not prohibit leveling. Having a high elastic modulus at high shear rates could potentially increase the initial film height of the applied paint and, according to Orchard's equation, should beneficially affect leveling behavior. Johansen reported that increasing $tan(\delta)$ values could lead to better leveling; however, Johansen did not provide analysis on this relationship.[46] It is likely that as the loss modulus dominates, the more fluid character dominates, thus allowing for better flow and leveling.

When correlating yield stress, the general trend of results validates expectations: higher yield stress values will prevent sag, which is expected to occur at low shear rates or stresses; however, too high of yield stress values will prevent adequate leveling. Eley found good logarithmic correlation of static yield stress values from a stress sweep to sag performance, where an increase in static yield stress values lead to better sag resistance.[7] Sarkar and Lalk found that a yield value of < 0.25 Pa for a sheared paint will lead to better leveling. Wu states that a yield stress < 1 dyn/cm^2 (0.1 Pa) will provide an acceptable sag and leveling balance.[47]

Lastly, there has been correlation to the rate of drying to sag and leveling performance. Since the paint will increase in viscosity as it dries due to higher solid content, it will resist sag and leveling. Molenaar *et al.* found that the longer it takes for the paint to reach maximum viscosity as it dries, the better the leveling and the worse sag will be.[48] Quach and Hansen found that the paint film will achieve poor leveling if the time it takes to reach a viscosity of 15 Pa is less than 50 seconds.[29]

1.4 Analytical Models for Sag and Leveling

Analytical models have been employed to better understand and describe the physical and rheological phenomenon behind sag and leveling. Leveling has been modeled as a sinusoidal wave in the Orchard equation where the amplitude of the wave diminishes over time as a corollary to the striations left by application diminishing over time. This equation, however, can only work in idealized cases. Orchard's later work attempting to develop a mathematical model accounting for surface tension and gravity and surface profile into a complex Fourier series could only be used for simple Newtonian fluids and failed to account for the complexities of paint drying and surface effects.[39] Murphy utilized a power law version of the Orchard equation that has been used by several works; however, this will often fail because the low shear stresses associated with sag and leveling fall outside of the power law regime.[49] Other researchers have also utilized mathematical simulations to better understand or predict leveling behavior. Much of the work done for sag and leveling simulations involves the use of a modified version of lubrication theory, a time-dependent solution of the Navier-Stokes equations that reduces the dimensionality and greatly increases the computational efficiency. Work done by Schwartz, Eres, Roy, Eley, and Weidner all use some version of the lubrication theory with some focus on a structure-changing effect like gravity, surface tension gradients, body forces, solvent loss, substrate geometry, or non-Newtonian flow behavior.[50–53] While useful, these numerical models are difficult to access. Therefore, an alternative approach is needed that can provide predictive capability for sag and leveling behavior that is readily accessible to paint formulators.

1.5   Introduction to Machine Learning

Machine learning is a subfield of artificial intelligence where algorithms "learn" patterns in data to make predictions or decisions for a specific task. Machine learning has been utilized in improving modern day-to-day life such as GPS navigation apps re-routing based on traffic patterns and the time of day, digital personal assistants learning voices to better understand and respond to requests, and online advertisements catering to personal tastes based on previous purchases or search histories. However, machine learning is also becoming a powerful tool to gain insights into scientific phenomena. Since there is little agreement on what rheological properties can influence or predict sag and leveling behavior, machine learning is a possible solution to create a model that predicts sag and leveling or to better understand the underlying mechanisms. Machine learning algorithms take data and fit that data a model. Once the model is "learned", new observations are added, and based on the new observations, predictions are made on that data. Machine learning algorithms can be categorized into supervised and unsupervised learning algorithms. Supervised learning algorithms use labeled data to make predictions. These supervised learning algorithms are often used for regression or classification tasks. Regression machine learning algorithms will take data and learn patterns in the data that output a continuous variable (i.e. sag or leveling ratings). Alternatively, machine learning algorithms can output categorical variables to classify groups. Unsupervised learning algorithms look at patterns in data that hint at some underlying structure.[54]

1.5.1   Generalized Additive Models

Generalized additive models (GAM) are a class of models that describe nonlinear relationships between the predictor variable and outcome as discrete weighted basis functions that are summed to form a final function. The weight of these simple basis

functions will determine how much it will contribute to the final function. These basis functions are often made up of piecewise polynomial functions known as splines that are separated by knots that divide the regions where the polynomials are fit. Figure 1.6 below shows how these basis functions are partitioned by splines and how these basis functions add to form the generalized additive model.
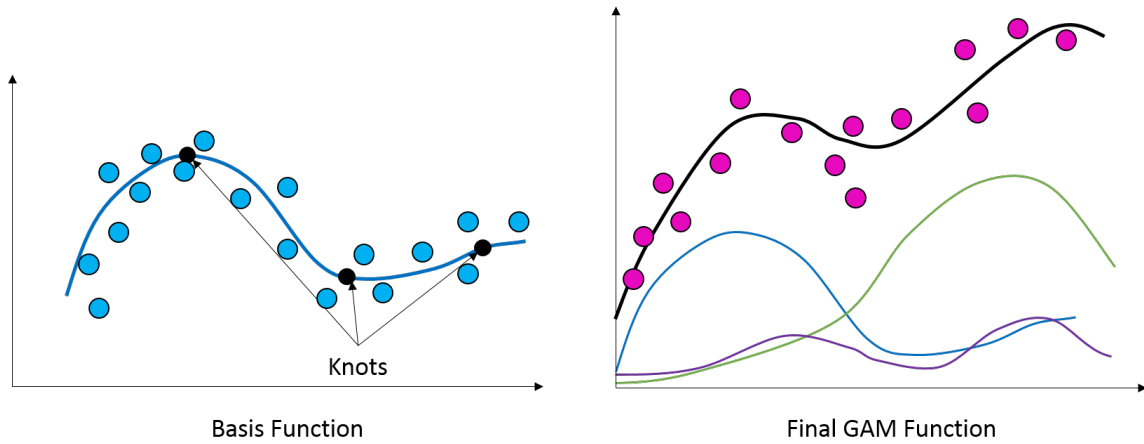
Figure 1.6: How basis functions are separated and how generalized additive models are formed from these basis functions.

The generalized additive model automatically selects the knots for spline functions, selects the weight of each basis function, and combines the basis functions of multiple predictor variables. However, GAMs may overfit the training set due to the flexibility in fitting nonlinear relationships and be poor at predicting data outside of the training dataset. The generalized additive model is shown below in Equation 1.18, where each $f(x)$ represents a function of some predictor variable, β_0 is the y-intercept, and ϵ is the unobserved error unaccounted for by the model.[54]

$$y = \beta_0 + f_1(x_1) + f_2(x_2) + ... f_k(x_k) + \epsilon \tag{1.18}$$

1.5.2   Regularization

One possible way of limiting overfitting of data is by regularization techniques such as LASSO (least absolute shrinkage and selection operator), ridge regression, and elastic net. Regularization techniques will shrink model parameters towards 0 that may be spurious predictors and force them to have little to no effect on predictions. These regularization functions are derivatives of the ordinary least squares (OLS) function which estimates parameters of a linear function by minimizing the squares of the differences of the observed dependent variable and that predicted by a linear function. The OLS function squares the calculated residuals for each combination of intercept and slope. The squared residuals are added up to give the sum of squares. The best fit model for OLS will be the function that minimizes this sum. The best fit models for LASSO and ridge regression are the models that minimize both the sum of squares and selecting the parameters that minimize the L1 or L2 penalty. The sum of squares loss function, which is the function that is minimized by the machine learning algorithm, is shown in Equation 1.19 below.

$$\sum_{i=0}^{n}(y_i - \hat{y}_i)^2 \tag{1.19}$$

LASSO adds an L1 norm function that is the sum of the absolute values of all parameter values multiplied by λ, a variable that penalizes model complexity at high values and is a hyperparameter that must be tuned for best performance by cross-validation. The L1 function is added to the OLS function to create the L1 loss function. The L1 function is able to shrink parameter values to 0, allowing for feature selection. However, there are limitations to LASSO: if there is a group of predictors that are correlated with each other, LASSO will only choose one of the predictors and LASSO is also unable to select more variables than there are cases. The L1 loss function is

described in Equation 1.20 below.

$$\sum_{i=0}^{n}(y_i - \hat{y}_i)^2 + \lambda \sum_{j=1}^{p}|\beta_j| \qquad (1.20)$$

Ridge regression adds an L2 norm function that is the sum of the squares of all parameter values multiplied by λ. The L2 norm function is added to the OLS function to create the L2 loss function. The L2 function can move parameter estimates towards 0, but will never reach 0, meaning it cannot provide feature selection. Ridge regression is useful if it is believed that all parameters will have some degree of predictive value. The L2 loss function is described in Equation 1.21 below.

$$\sum_{i=0}^{n}(y_i - \hat{y}_i)^2 + \lambda \sum_{j=1}^{p}\beta_j^2 \qquad (1.21)$$

Elastic net linearly combines L2 and L1 regularization and finds a combination of parameter estimates somewhere between those found by ridge regression and LASSO using the tunable hyperparameter α, which can take any value between 1 (which will result in LASSO) and 0 (which will result in ridge regression). Elastic net can circumvent both problems of LASSO and can perform feature selection unlike ridge regression.[54] The elastic net loss function is described in Equation 1.22 below.
Elastic Net Loss Function

$$\sum_{i=0}^{n}(y_i - \hat{y}_i)^2 + \lambda((1-\alpha)\sum_{j=1}^{p}\beta_j^2 + \alpha\sum_{j=1}^{p}|\beta_j|) \qquad (1.22)$$

1.6   Purpose of Study

In this study, generalized additive models are used to quantify a relationship between rheological parameters and sag and leveling measures for formulated paints with dis-

tinct rheological profiles. Formulation data from the paint could then be used to provide predictive capabilities for its rheological behavior and thus sag and leveling performance. To this end, a predictive model of sag and leveling performance could be utilized to provide accurate analysis of end-use performance based on formulation data alone.

1.7 Limitations and Considerations

Due to the recent COVID-19 outbreak, access to lab facilities was limited and insufficient data was collected to fulfill the stated objective of the thesis; however, the results appear to be promising and yielded potentially deeper insight into sag behavior.

Chapter 2

METHODS AND MATERIALS

In total, twelve waterborne interior architectural paints were made. Four "original" paints (825, 2020, 100% XG, and 100% HEC) were made using the formulations provided in Appendix A in two parts: first, in the grind phase, pigments and other grind phase components are mixed at 2000 rpm to disperse the pigment; second, the grind is mixed with latex resins and other letdown components in the letdown phase to create the formulated paint. A sample formulation is shown below in Figure 2.1. All materials were used as supplied with no further modification. The 825, all XG designated paints, and all HEC designated paints were formulated to include 1 wt.% of Acrysol RM-2020, a urethane associative thickener. The 2020 paint is primarily thickened with only RM-2020. The 825 paint is primarily thickened with Acrysol RM-825, a non-ionic urethane rheology modifier, while the XG paints were primarily thickened with a 2% solution of xanthan gum and the HEC paints were primarily thickened with a 2% solution of Natrosol 250 HR, a 2.5 molar substituted hydrox-yethyl ether cellulose thickener. The four original paints were formulated to have an approximate pigment volume concentration (PVC) of 20 and adjusted to reach an approximate viscosity of 90 KU with the primary rheological modifier. KU viscosity measurements were performed with a Brookfield KU-2 viscometer. Paints formulated for the XG and HEC "ladder" were calculated to contain 10-90% of the mass of the primary thickener in 10% increments, with all else constant except for the missing weight of the thickener solutions which was substituted with water. The "ladder" paints were formulated from a 10x batch of the original 100% formulation, without the primary thickener in the grind or letdown or water in the letdown. Otherwise, the mother batches were produced in the same manner as the four original paints. The

mother batch was equally divided by weight between nine paint cans and each can had the appropriate amount of thickener added. The formulation data is provided in Appendix A.

		20 PVC with TiO2	Architectural Acrylic Paint			
GRIND:						
			Formula		**Non-Volatile**	
% NV	**Lbs/Gal**	**Material**	**Lbs**	**Gal**	**Lbs**	**Gal**
0	8.33	Water	55.08	6.61	0.00	0.00
25	9.19	Tamol 731A	5.75	0.63	1.44	0.11
98	8.35	BYK 022	0.19	0.02	0.19	0.02
1.5	7.18	Kathon LX 1.5%	0.23	0.03	0.00	0.00
25	8.26	Acrysol RM-2020	4.00	0.48	1.00	0.12
2	8.32	2% Natrosol 250 HI	20.00	2.41	0.40	0.05
100	33.33	Ti-Pure R-902	83.71	2.51	83.71	2.51
0	8.66	Propylene Glycol	3.61	0.42	0.00	0.00
70	8.91	Tergitol 15-S-40	4.00	0.45	2.80	0.31
Grind Total			176.57	13.56	89.54	3.14
Pigment Total			83.71	2.51	83.71	2.51
Grind (2000 rpm) to Hegman 7+						
LETDOWN:						
			Formula		**Non-Volatile**	
% NV	**Lbs/Gal**	**Material**	**Lbs**	**Gal**	**Lbs**	**Gal**
		Grind	176.57	13.56	89.54	3.14
0	8.33	Water	0.00	0.00	0.00	0.00
98	8.35	BYK 022	0.20	0.02	0.20	0.02
50	8.82	Rhoplex SG 30	176.44	20.01	88.22	9.42
2	8.32	2% Natrosol 250 HI	41.92	5.04	0.84	0.11
0	8.33	Water	0.00	0.00	0.00	0.00
0	7.93	Texanol	4.87	0.61	0.00	0.00
TOTAL			400.00	39.25	178.79	12.69
Paint properties						
Weight per gallon		10.19				
Viscosity						
% NV by weight		44.70				
% NV by volume		32.32				
PVC		19.80				

Figure 2.1: Sample formulation of the 100% HEC paint

All paints were characterized using rheological data acquired from a TA Instruments Discovery HR-2 Hybrid Rheometer through three tests: a flow sweep from 0.01 s^{-1} to 1000 s^{-1} at 25°C, an amplitude sweep from 0.01% to 100% strain at 1.0 Hz and 25°C, and a frequency sweep from 0.01 to 100 Hz at 1% strain and 25°C. Yield stress values were determined from amplitude sweeps by calculating the last point in the storage modulus (G') that separates the linear viscoelastic region plateau and the sloping nonlinear viscoelastic region. The point is determined using the onset point function in the TA Instruments TRIOS software (ver. 5.1.0.46403).

Sag tests were done following ASTM D4400-18 with Gardner Co. Leneta Anti-Sag Meters ASM-1 and ASM-4 and given a sag rating as described in the introduction.[18] Leveling tests were done following ASTM D4062-11 with a BYK-Gardner 0813 Leveling Test Blade and given a leveling rating from 0 (poor leveling) to 10 (perfect leveling or no perceptible ridges) using four separate individuals to evaluate the leveling rating in lieu of a leveling standard.[2] Leveling values were not able to be recorded for the XG and HEC ladders and sag values could not be obtained for the 80%, 60%, 40%, and 20% XG and HEC paints.

Chapter 3

RESULTS AND DISCUSSION

3.1 Rheological Characterization

The concentrations of the rheological modifiers in all four paints are summarized in Table 3.1.

Table 3.1: Rheological Modifier Concentrations of the Four "Original" Paints

Formulation	Acrysol RM-2020 (wt. %)	Acrysol RM-825 (wt. %)	Xanthan Gum (wt. %)	Natrosol 250 HR (wt. %)
2020	7.64			
825	1	0.83		
XG	1		0.32	
HEC	1			0.31

The final KU viscosities of the "original" four formulated paints are summarized in Table 3.2 below.

Table 3.2: Final KUs of the Four "Original" Paints

Formulation	Final KU
2020	88.2
825	92.7
XG	82.7
HEC	86.3

The HEC and xanthan gum formulations proved difficult to reach a KU viscosity of 90; all the water in the letdown and some of the water in the grind were substituted with a 2% solution of the respective thickener. However, these paints were not intended to replicate real world formulations, but to create paints with defined rheological profiles that are distinct from formulation to formulation, while keeping the

viscosity as close to the industry standard of 90 KU as possible. The 825 formulation required very little of the thickener to reach the goal of approximately 90 KU and the 2020 formulation required significantly more thickener to reach around 90 KU but did not necessitate displacing water in the formulation. No KU measurements were utilized for the ladder paints, but the KU of these paints are expected to be lower than their 100% counterparts.

All paints were subjected to a flow sweep on the rheometer at 25°C, with an increase in shear rate from 0.01 s^{-1} to 1000 s^{-1}. It is expected for the xanthan gum thickened paint to have the highest yield stress followed by the HEC thickened paint, the 2020 paint was expected to have the next highest yield stress, followed by the 825 paint with Newtonian behavior and very low yield stress. The results are summarized in Figure 3.1 below.
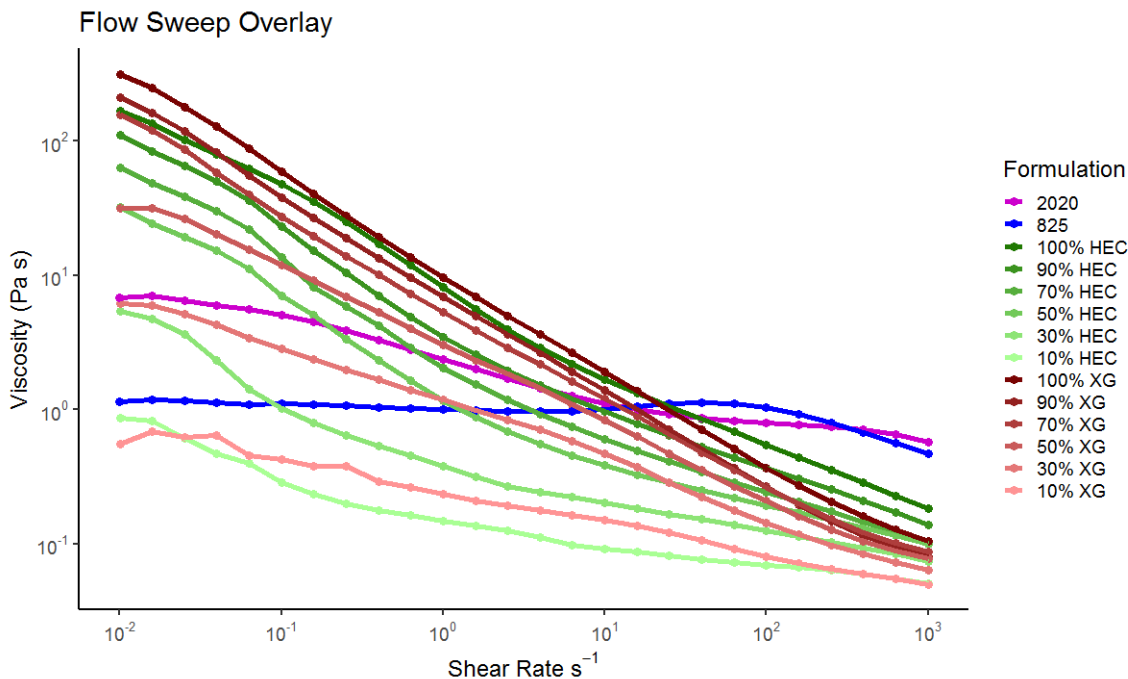
Figure 3.1: Flow sweep of all paint formulations.

From the flow sweep, all four "original" paints show distinct rheological profiles, with both xanthan gum and HEC displaying shear-thinning with high yield stress,

2020 displaying Newtonian behavior with a yield stress, and 825 showing nearly New-tonian behavior, with a slight shear-thickening hump leading into shear thinning at high shear rates. As expected, the viscosity decreases as the concentration of the thickener decreases as well as becoming less shear-thinning in character. The paints were then subjected to an amplitude sweep at 25°C consisting of 1.0 Hz frequency and an increase in strain from 0.01% to 100%. The results of the amplitude sweep are summarized in Figures 3.2, 3.3, and 3.4 below.
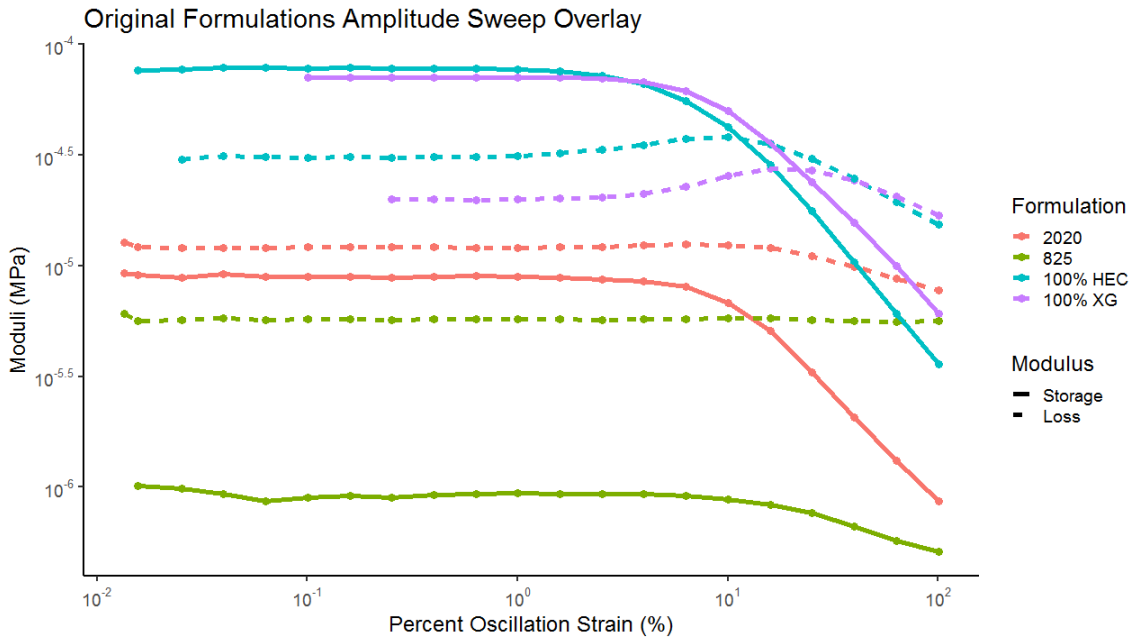
Figure 3.2: Amplitude sweep of the four "original" paints.
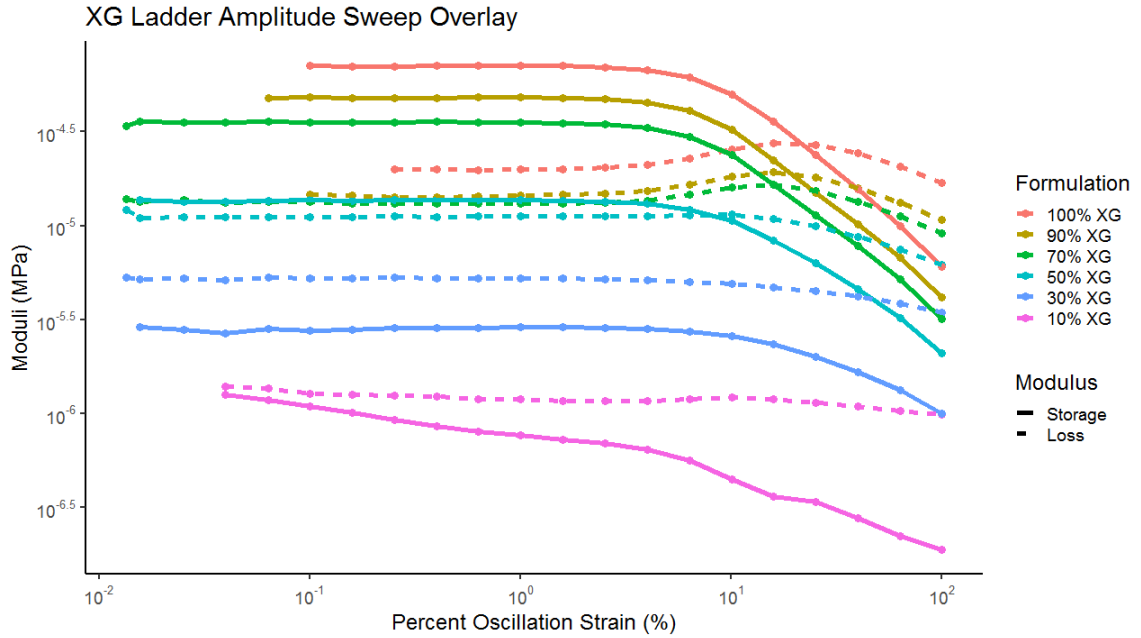
Figure 3.3: Amplitude sweep of the XG ladder.
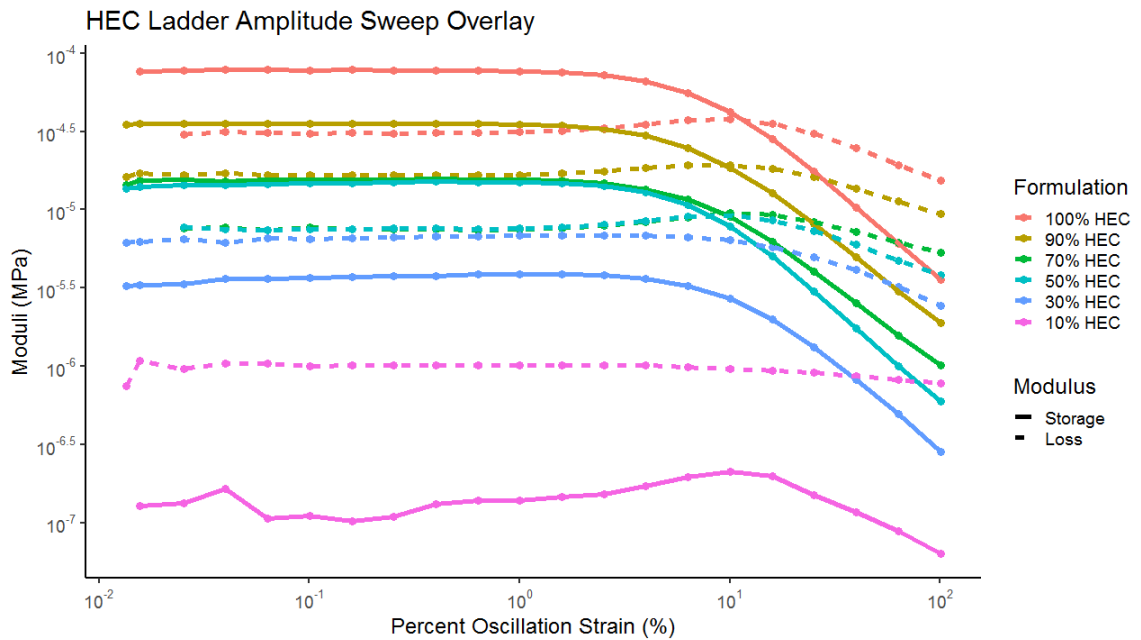
Figure 3.4: Amplitude sweep of the HEC ladder.

The XG and HEC paints both display higher storage moduli compared to the loss moduli. The opposite is true for both 825 and 2020 formulations. This indicates

that the long chains of the polysaccharide xanthan gum and cellulosic HEC allow for more energy to be stored within the structure. This is expected to lead to better sag resistance, but worse leveling as the structure present in these formulations will prevent flow, as noted by the high yield stress data gathered from the amplitude sweeps below. Both samples have the loss moduli dominate at high oscillation strains, indicating that the structure is broken up and the viscous portion of the material dominates. Conversely, both the 825 and 2020 formulations have the viscous portion dominate at all strains, with 825 showing no change in G'' and a near constant G', reflecting its nearly Newtonian character. Yield stress values determined from the amplitude sweep are summarized in Table 3.3 below.

Table 3.3: Static Yield Stress Values

Formulation	Static Yield Stress (Pa)
2020	0.711
825	0.325
100% XG	1.359
90% XG	0.739
70% XG	0.533
50% XG	0.235
30% XG	0.130
10% XG	0.047
100% HEC	0.805
90% HEC	0.450
70% HEC	0.332
50% HEC	0.307
30% HEC	0.254
10% HEC	0.083

The paints were subjected to a frequency sweep at 25°C at 1% strain and an increase in frequency from 0.01 to 100 Hz. The results are summarized in the Figures 3.5, 3.6, and 3.7 below.
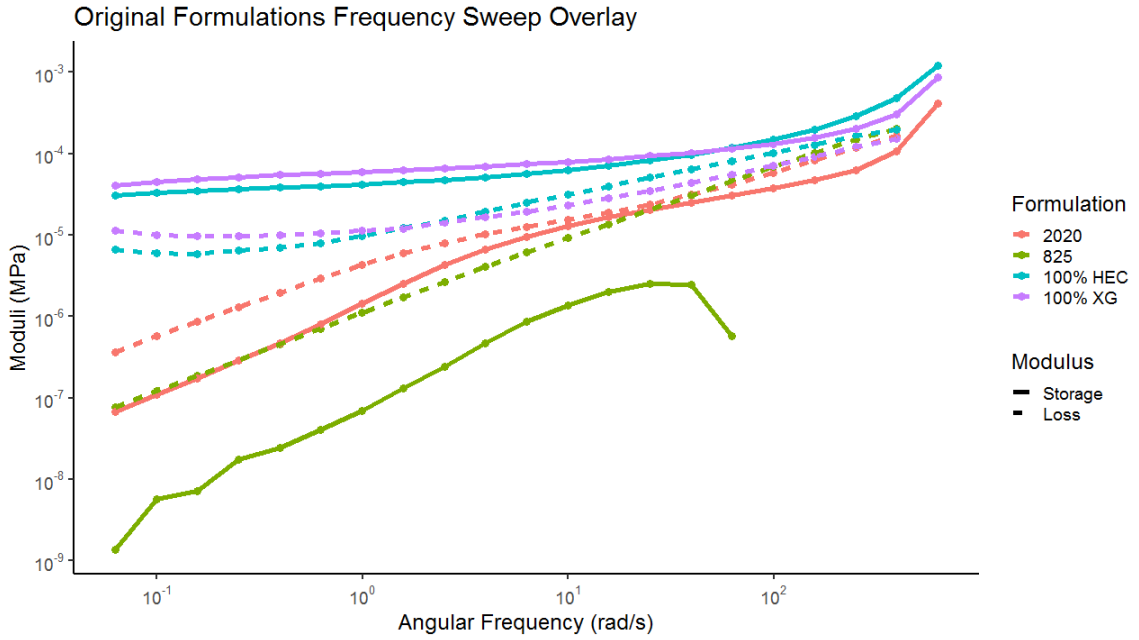
Figure 3.5: Frequency sweep of the four "original" paints.
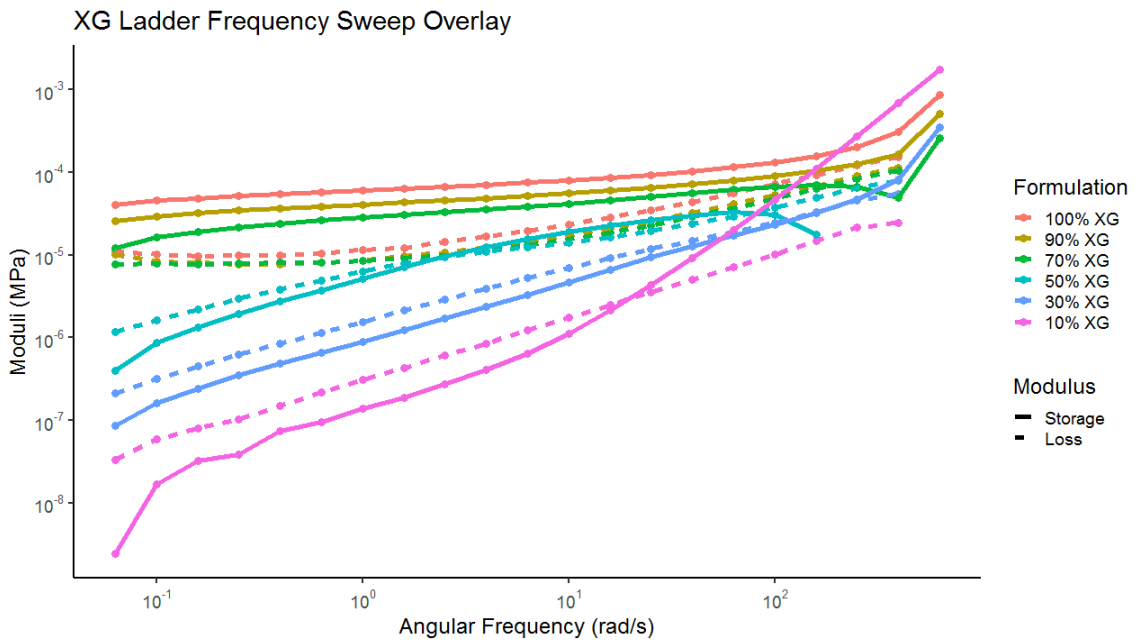
Figure 3.6: Frequency sweep of the XG ladder.
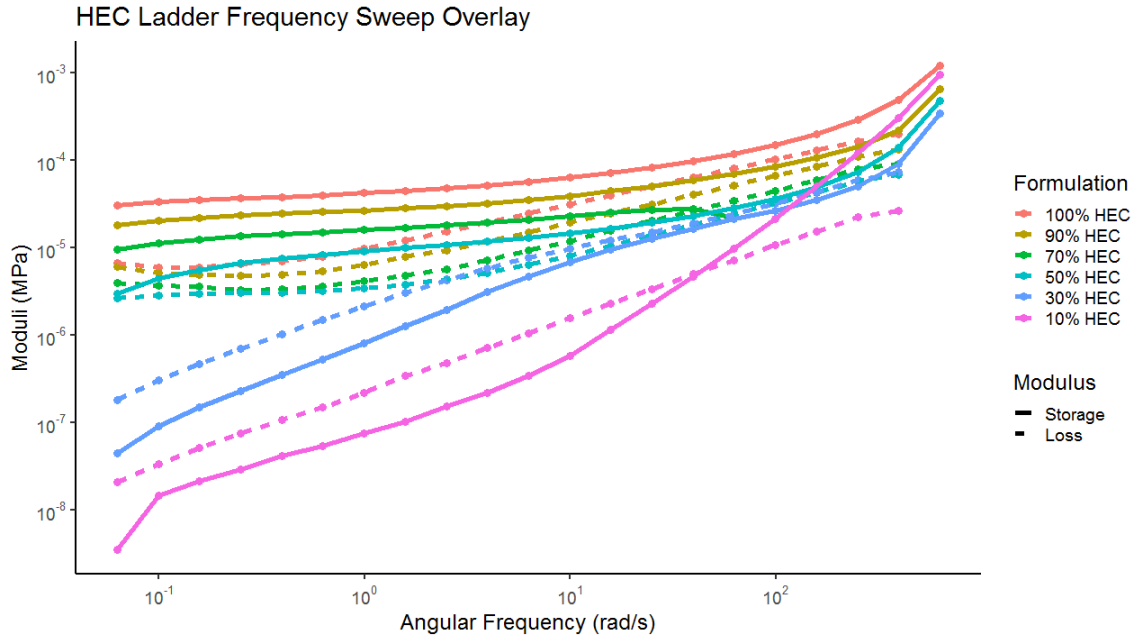
Figure 3.7: Frequency sweep of the HEC ladder.

The results of the frequency sweep reaffirm the moduli seen in the amplitude sweep; however, in literature there is little relevance of the frequency sweep to sag and leveling considerations. Lu did find a logarithmic correlation of loss modulus to leveling at a frequency sweep albeit at 35% strain, which at low frequencies is indicative of sag and leveling behavior.[45]

3.2 GAM Analysis

Using a generalized additive model (GAM) to run nonlinear regression on the entire breadth of rheological data for all paints to predict sag behavior yielded interesting results. The GAM code does utilize feature selection to select the most informative predictors from the rheological data gathered.
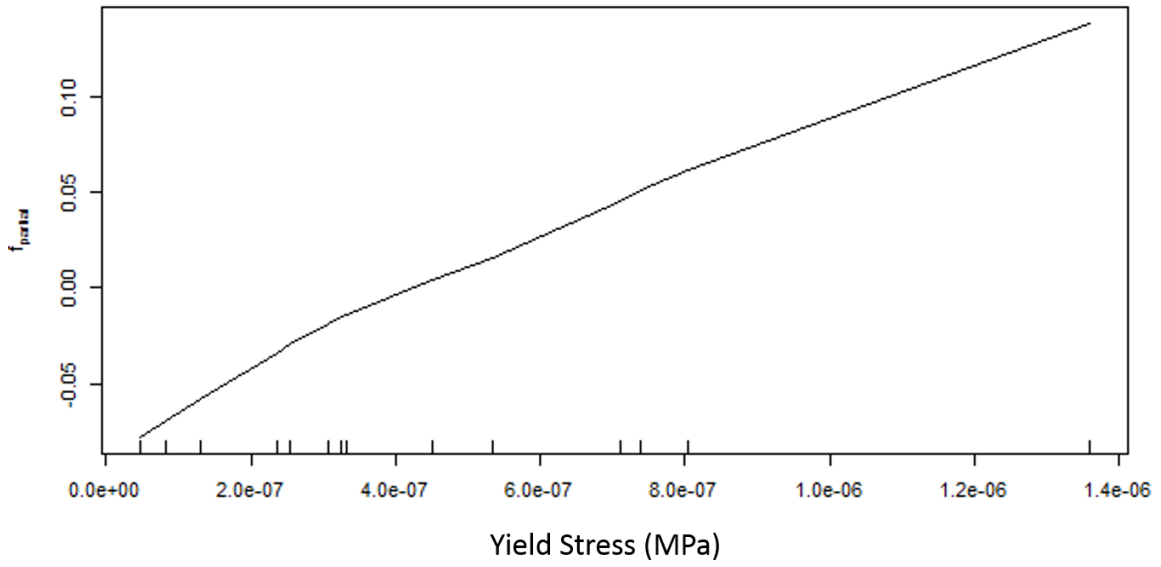
Figure 3.8: Yield stress selected by GAM without regularization.
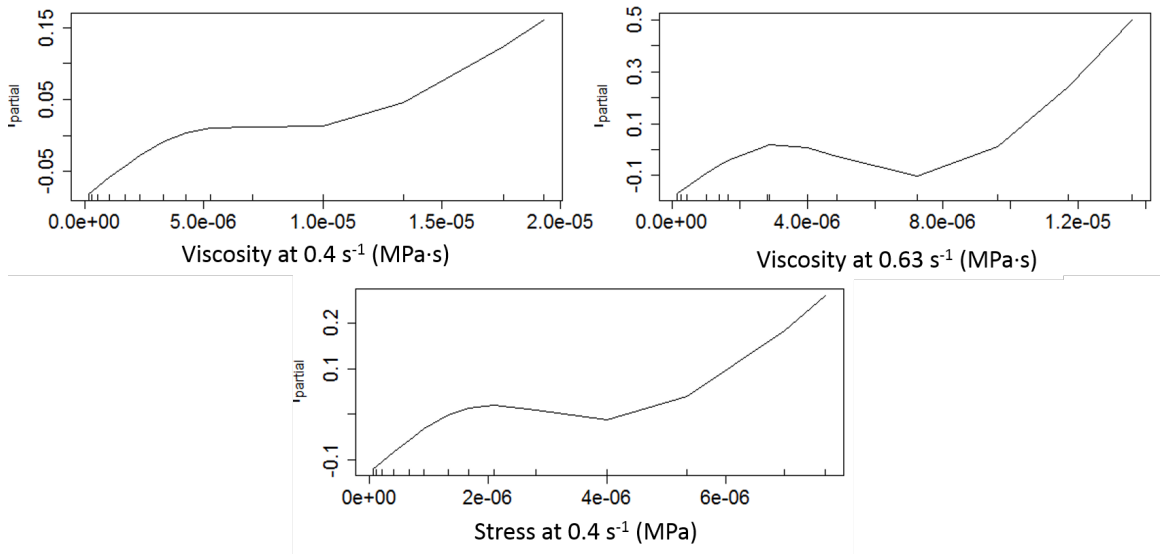
Figure 3.9: Low-shear parameters selected by GAM without regularization.

The results of GAM show some expected results: viscosities at low shear rates of 0.4 and 0.63 s^{-1} as well as stress at 0.4 s^{-1} and the static yield stress do influence sag behavior. The GAM partial effects on the y-axis, which show how much that parameter with that specific value will increase or decrease the sag rating according

to the partial effect value, also agree with previous knowledge: increasing yield stresses increase sag resistance while low viscosity at low shear rates or stresses tend to have a negative effect on sag resistance and higher viscosities at these rates or stresses increase sag resistance. It is interesting to note that increased storage moduli at a low frequency of 0.06 rad/s, which simulates slow motion at long timescales, appears to play a fairly significant role in sag behavior, with nearly ten times the partial effect of yield stress. The curves of both the storage moduli and yield stress curves are similar and much like the yield stress, could indicate the amount of structure present to resist sag flow at low stresses and long timescales.

However, there are unexpected results. Mid-shear stresses at 160, 250, and 630 s^{-1} appear to have an influence on sag behavior.
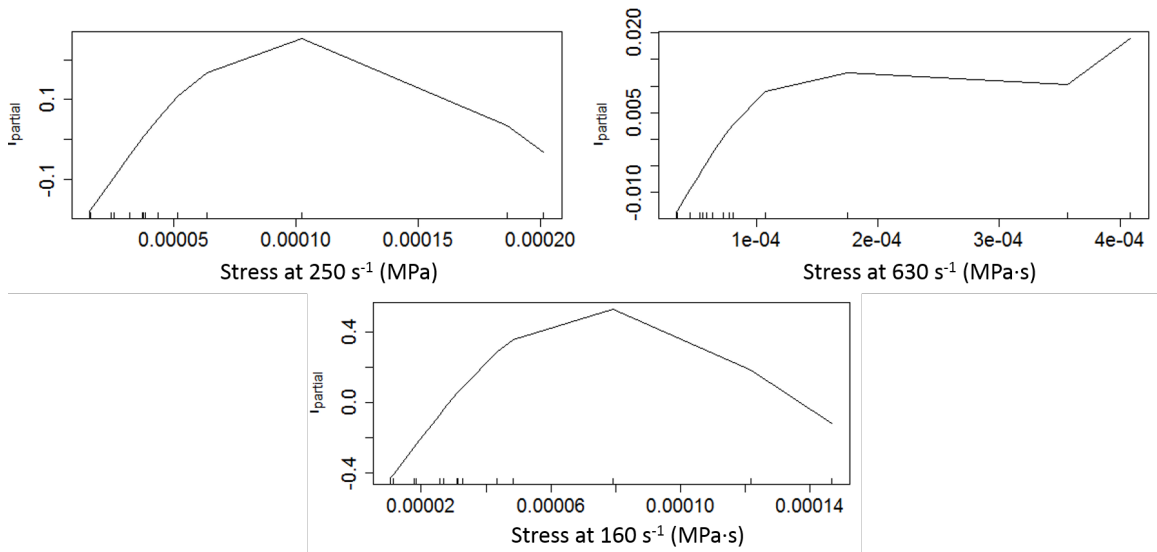
Figure 3.10: Mid-shear parameters selected by GAM without regularization.

There have been no literature precedents of mid-shear stresses having an influence in sag and axiomatic knowledge of sag and leveling behavior should expect sag and leveling to be dictated by low shear rate or stress flow. However, Eley did state that the initial film geometry could possibly be dictated by a shear rate or stress

process that is lower than the application shear rate or stress. Eley also found linear correlation between brushmark frequency and viscosity between 50 to 200 dyn/cm^2, which, for the paints studied, is near the mid-shear rates of interest.[5] It could be possible that the initial film geometry could have more of an influence on sag behavior than previously thought. Further supporting this theory is the presence of normal stress (N1) having an influence on sag behavior, again at these mid-shear rates of 400 and 630 s^{-1} (Figure 3.11).
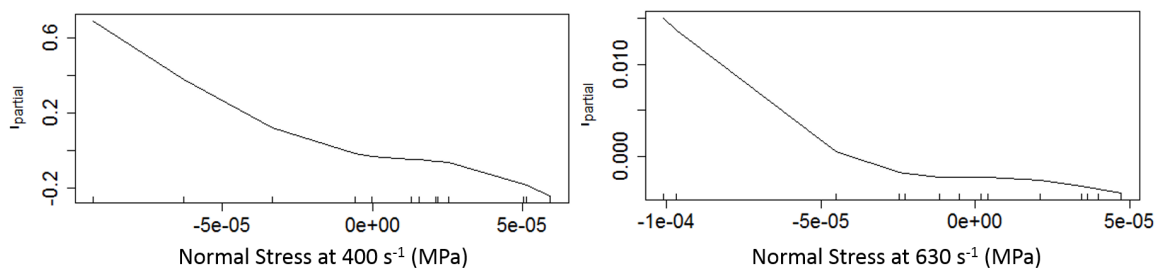
Figure 3.11: Normal forces selected by GAM without regularization.

From the paper by Chatterjee *et al.*, they state that brush drag is likely worsened or helped by the normal forces resulting from the normal stress differences during application.[17] These forces could potentially increase the initial film geometry during application which could positively affect leveling (based on Orchard's equation) or negatively affect sag, where the evaporative flux due to the increased height allows for more time for gravity to act on the peak or for surface tension gradients to arise from uneven drying. This seems to correlate well with the partial effects of the normal stresses; negative normal stresses seem to positively affect the sag model, where a thinner film could be formed as a result of increased brush contact due to the normal force, while negatively affecting the model with positive normal stresses, where less brush contact could yield increased film heights. However, without leveling data, it is difficult to discern if this relationship holds true. Furthermore, the limited amount of data gathered also constrains the extent of these conclusions. The normal

Q-Q plots show a fairly normal distribution of data; however, the amount of data points for stresses at these mid-shear regions dwindles down to one or two points that show a neutral or negative relation to sag at higher values of stress. Therefore, no firm conclusions can be drawn from the data. Also, due to the focus on shear rate as an independent variable in sag and leveling behavior, there is little research focused on oscillation strains or frequencies relating to sag and leveling. It is also entirely possible that any predictors selected may be selected out of a purely coincidental relationship with sag and leveling measures or the data may be overfit through these spurious predictors.
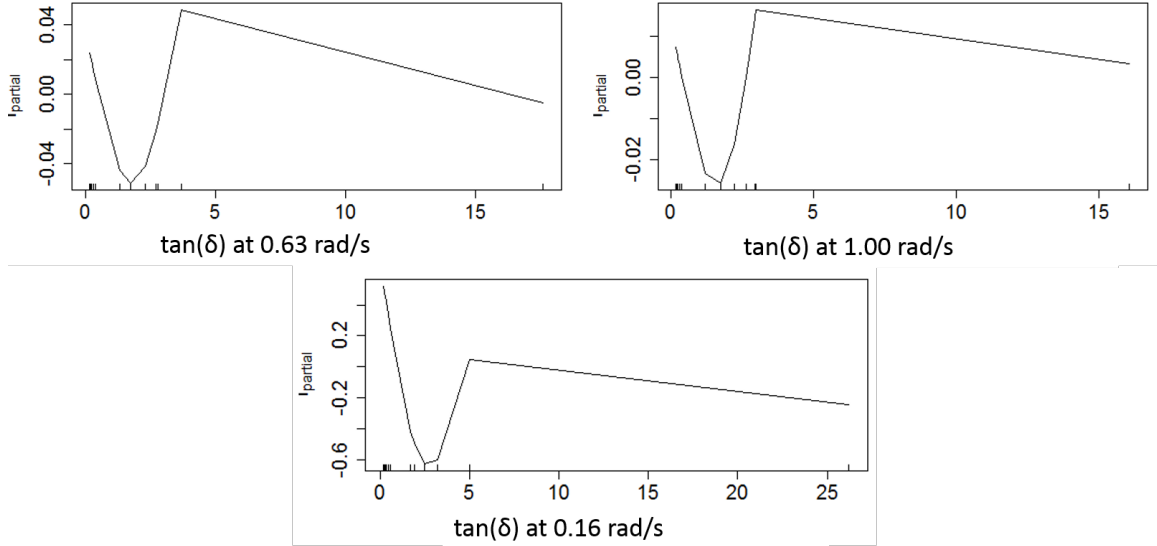
Figure 3.12: $\tan(\delta)$ **parameters selected by GAM without regularization.**

Based on the results shown in Figure 3.12, that may be the case. The $\tan(\delta)$ values, while at low angular frequencies that may be associated with sag, contain an outlier at high values of $\tan(\delta)$ that will constrain the predictive capabilities of the model that may have $\tan(\delta)$ values that lie between. An alternative approach is to apply regularization on the rheological data beforehand through elastic net, then run a GAM algorithm on the top 20 predictors, which would further trim the amount of predictors. This method will help reduce overfitting and hopefully provide predictors

that are more relevant to sag and leveling behavior. The results of the elastic net are shown in Figure 3.13 below.
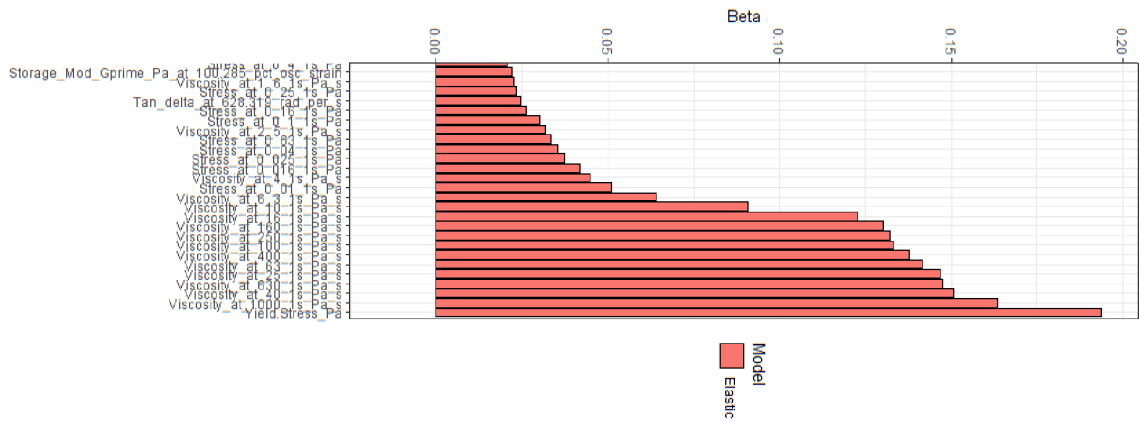
Figure 3.13: Elastic net results without regularization.

Interestingly, low shear viscosities and stresses appear to have less effect than high and mid-shear viscosities. However, running a GAM algorithm on the remaining predictors will provide better insight to sag and leveling behavior. The results are summarized in the Figures 3.14, 3.15, and 3.16 below.
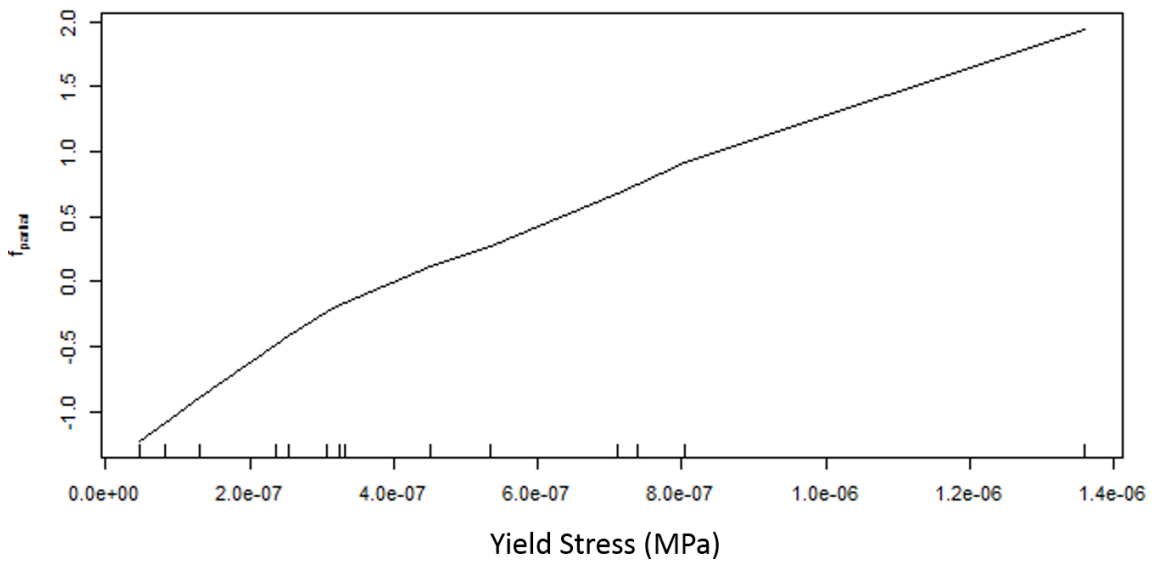
Figure 3.14: GAM results with elastic net regularization.

Figure 3.15: GAM results with elastic net regularization.

Figure 3.16: GAM results with elastic net regularization.

The results reaffirm the role that yield stress and low shear stress have on sag, although low shear viscosity is notably absent, save for viscosity at 6.3 s^{-1}. It could be possible that utilizing a stress-controlled experiment to measure viscosity may yield more relevant results for a larger range of paints. It would be worthwhile to see if utilizing shear stress-controlled experiments would yield better predictive capabilities than the current shear rate-controlled method. Interestingly, consecutive mid-shear

viscosities at 160, 250, and 400 s^{-1} are shown to have an influence on sag and leveling behavior. Based on these results and the previous GAM algorithm, it is possible that this is a shear rate range of interest for initial film geometry. Based on these curves, it appears that there is some ideal viscosity at these mid-shear rates. A possible explanation is that too low of a viscosity will cause the paint to readily flow after application while too high of a viscosity will cause a high frequency of brushstrokes or too high of a film to form and sag will occur as a result of the unevenness of the film.
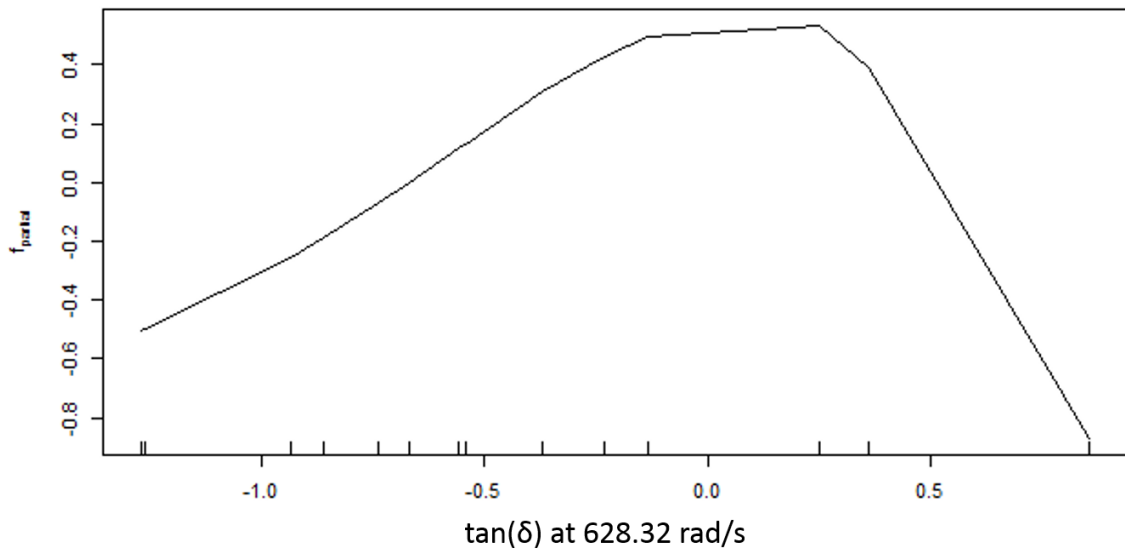
Figure 3.17: tan(δ) at 628 rad/s

Lastly, tan(δ) at 628 rad/s, which relates to fast motion at short timescales, could be indicative of the amount of energy dissipation at application. It appears that too low or too high of a tan(δ) negatively affects sagging performance. However, the implications of these results are not well-understood. Having a tan(δ) of 0, would mean that the phase angle would equal 0 and an ideally elastic response is preferred during fast motion at these short timescales. A possible explanation could be that instant deformation at application is preferred to be spread easily and evenly across the substrate, minimizing the amount of defects and improving both sag and leveling.

More data is necessary to create a full picture of the effects of $\tan(\delta)$ at high oscillation frequencies, mid-shear viscosities, and comparisons of utilizing low shear rates or stresses in the model.
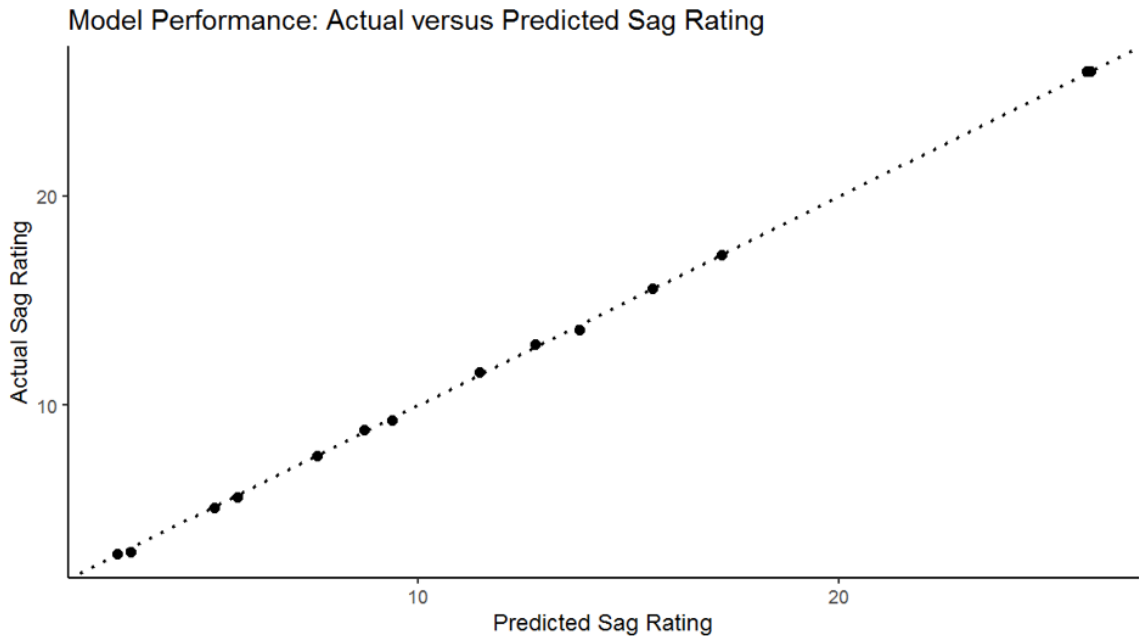
Figure 3.18: Actual vs. Predicted Sag Ratings Generated by the GAM Model.

The predicted vs. actuals plot (Figure 3.18) shows a model that can nearly perfect predict the sag rating based on the rheological parameters discussed earlier. However, it is possible that the model has severely overfit the data, but it is not possible to determine if this is the case without applying a new formulation to the model. The rheological parameters the model chose are justifiable and should be applicable to a variety of formulations; however, more data is necessary. The benefit to utilizing this machine learning algorithm is that it is amenable to future data and will invariably improve the model with each iteration. The normal Q-Q plots (Figure 3.19) also show a non-normal distribution of data points, requiring more data to be gathered to make more conclusive interpretations.
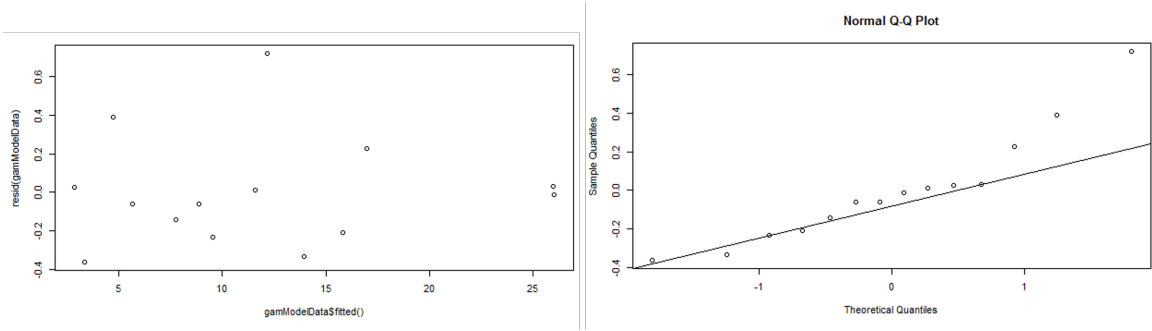
Figure 3.19: Residuals vs. Fitted and Normal Q-Q Plot of the Elastic Net Regularized Model

Chapter 4

CONCLUSIONS AND FUTURE DIRECTIONS

Due to the limited amount of lab access, the data collected is woefully incomplete; however, based on analysis of the data available, it appears that viscosity or stress at mid-shear rates has more of an effect on sag behavior than previously thought. This is likely due to the initial film geometry being formed at shear rates lower than the application shear rates as stated by Eley.[5] Furthermore, static yield stress and stresses at low shear rates predictably affect sag. However, there is dispute as to whether the current shear rate approach is sufficient to predict sag and leveling behavior. There is a benefit to using shear stress as vector components of surface tension, gravitational, body, and centrifugal forces can be incorporated into shear stress values, as shear rates are not independent of rheology.

Paramount work will involve verifying the model based on rheological data from a paint the model has not been exposed to. Future work will include collecting data on the entire ladder of thickener dilutions as well as formulating ladders for 2020 and 825 paint bases. Leveling data will also need to be collected, as it will be indicative of validity of the mid-shear stress/rate explanation. GAM will be run on the leveling data, using the same elastic net regularized data. If this explanation is to be true, it would be expected that leveling would be positively affected by increasing viscosity within these mid-shear ranges. These increasing viscosities will correlate to brushmark frequencies and since the brushmark frequencies are proportional to the wavelength and thus the rate of leveling based on Orchard's equation, a positive correlation between increasing mid-shear viscosities and leveling is expected. Lastly, it would be useful to utilize a controlled-stress flow sweep to compare along the controlled-shear-rate flow sweeps that were previously run. Based on the GAM results, there

can sometimes be disagreement as to whether stress or viscosity at shear rates of interest should be utilized in the model. Since shear rates and shear stresses could both potentially be used to calculate viscosity, it would be useful to utilize them separately in two different models then use those models to predict the sag and leveling behavior of a paint the models have not been exposed to. This could either prove the superiority of utilizing shear stress or may prove that the current shear rate methodology is sufficient to predict sag and leveling.

While there has been no validation of the accuracy of this model, the interpretability of the model does provide insight into the significance mid-shear viscosities may have on sag performance as well as verifying previous notions. The model is amenable to future data that future students may collect and will improve the predictive capabilities of the model as well as potentially finding other correlations that previous researchers may have missed. The preliminary results are promising, but the scope of this work was limited by factors that could not be controlled.

REFERENCES

1. Whittingstall, P. Paint evaluation using rheology. *TA Instruments Publication Rh059, downloaded from http://www. tainstruments. com/library_download. aspx* **2011**.

2. *Standard Test Method for Leveling of Paints by Draw-Down Method*; Standard; West Conshohocken, PA: ASTM International, 2016.

3. Saranjam, N.; Chandra, S.; Mostaghimi, J.; Fan, H.; Simmer, J. Orange peel formation due to surface tension-driven flows within drying paint films. *Journal of Coatings Technology and Research* **2016**, *13*, 413–426.

4. Evans, P.; Schwartz, L.; Roy, R. A mathematical model for crater defect formation in a drying paint layer. *Journal of colloid and interface science* **2000**, *227*, 191–205.

5. Eley, R. R. Applied rheology and architectural coating performance. *Journal of Coatings Technology and Research* **2019**, *16*, 263–305.

6. Smith, K.; Barsotti, R.; Bell, G. In *Proceedings of the XIVth International Conference on Organic Coatings Science and Technology, Athens, Greece*, 1988, pp 315–331.

7. Eley, R. R. Applied rheology in the protective and decorative coatings industry. *Rheology Reviews* **2005**, *2005*, 173.

8. Lambourne, R.; Strivens, T. A., *Paint and surface coatings: theory and practice*; Elsevier: 1999.

9. Espin, L.; Kumar, S. Sagging of evaporating droplets of colloidal suspensions on inclined substrates. *Langmuir* **2014**, *30*, 11966–11974.

10. Weidner, D. E. Leveling of a model paint film with a yield stress. *Journal of Coatings Technology and Research* **2020**.

11. Overdiep, W. The levelling of paints. *Progress in organic coatings* **1986**, *14*, 159–175.

12. Understanding yield stress measurements, 2012.

13. Tadros, T. F., *Rheology of dispersions: principles and applications*; John Wiley & Sons: 2011.

14. Koerner, M. R. In *Protective Coatings*; Springer: 2017, pp 95–113.

15. Bhavsar, R.; Shreepathi, S. Evolving empirical rheological limits to predict flow-levelling and sag resistance of waterborne architectural paints. *Progress in Organic Coatings* **2016**, *101*, 15–23.

16. Kornum, L.; Nielsen, H. R. Surface defects in drying paint films. *Progress in Organic Coatings* **1980**, *8*, 275–324.

17. Chatterjee, T.; Linsen, M.; Ginzburg, V. V.; Saucy, D. A.; Nakatani, A. I.; Van Dyk, A. K. Influence of the first normal stress differences on model hydrophobically modified ethoxylated urethane-thickened waterborne paints brush drag. *Progress in Organic Coatings* **2019**, *135*, 582–590.

18. *Standard Test Method for Resistance of Paints Using a Multinotch Applicator*; Standard; West Conshohocken, PA: ASTM International, 2018.

19. Deka, A.; Dey, N. Rheological studies of two component high build epoxy and polyurethane based high performance coatings. *Journal of Coatings Technology and Research* **2013**, *10*, 305–315.

20. Mezger, T. G., *The rheology handbook: for users of rotational and oscillatory rheometers*; Vincentz Network GmbH & Co KG: 2006.

21. Barnes, H. A. The 'yield stress myth?'paper–21 years on. *Applied Rheology* **2007**, *17*, 43110–1.

22. Garakani, A. K.; Mostoufi, N.; Sadeghi, F.; Fatourechi, H.; Sarrafzadeh, M.; Mehrnia, M., et al. Comparison between different models for rheological characterization of activated sludge. *Journal of Environmental Health Science & Engineering* **2011**, *8*, 255–264.

23. Raju, K.; Krishna, D.; Devi, G. R.; Reddy, P.; Yaseen, M. Assessment of applicability of carreau, ellis, and cross models to the viscosity data of resin solutions. *Journal of applied polymer science* **1993**, *48*, 2101–2112.

24. Fernandes, R. R.; Andrade, D. E.; Franco, A. T.; Negrao, C. O. The yielding and the linear-to-nonlinear viscoelastic transition of an elastoviscoplastic material. *Journal of Rheology* **2017**, *61*, 893–903.

25. Dinkgreve, M.; Paredes, J.; Denn, M. M.; Bonn, D. On different ways of measuring "the" yield stress. *Journal of non-Newtonian fluid mechanics* **2016**, *238*, 233–241.

26. Barnes, H. A. The yield stress—a review or '$\pi\alpha\nu\tau\alpha$ $\rho\varepsilon\iota$'—everything flows? *Journal of Non-Newtonian Fluid Mechanics* **1999**, *81*, 133–178.

27. Barnes, H.; Walters, K. The yield stress myth? *Rheologica acta* **1985**, *24*, 323–326.

28. Macosko, C. W. Rheology Principles. *Measurements and Applications* **1994**.

29. Quach, A.; Hansen, C. Evaluation of leveling characteristics of some latex paints. *Journal of Paint Technology* **1974**, *46*, 40–46.

30. Khanna, R. Rheological factors affecting brush marks in gloss emulsion paints. *Paint Technol* **1969**, *33*, 23–34.

31. Wu, S. Rheology of high solid coatings. I. Analysis of sagging and slumping. *Journal of Applied Polymer Science* **1978**, *22*, 2769–2782.

32. Dodge, J. S. Quantitative measures of leveling. *Journal of Paint Technology* **1972**, *44*, 72.

33. Deka, H.; Karak, N. Epoxy Modified Bio-based Hyper branched Polyurethane/-Clay Nanocomposites: Rheology and Biodegradability. *Journal of NanoScience, NanoEngineering & Applications* **2013**, *3*, 1–12.

34. Colclough ML, S. N.; TA, W. A Low Shear Viscometer: An Instrument for Measuring Flow and Sag Resistance in Coatings. *Journal of the Oil and Colour Chemists' Association* **1980**, *63*, 183–193.

35. Meyers, M. A.; Chawla, K. K., *Mechanical behavior of materials*; Cambridge university press: 2008.

36. Franck, A.; Germany, T. I. Viscoelasticity and dynamic mechanical testing. *TA Instruments, New Castle, DE, USA AN004* **1993**.

37. Castro, M.; Giles, D. W.; Macosko, C.; Moaddel, T. Comparison of methods to measure yield stress of soft solids. *Journal of Rheology* **2010**, *54*, 81–94.

38. Banfill, P.; Saunders, D. On the viscometric examination of cement pastes. *Cement and Concrete Research* **1981**, *11*, 363–370.

39. Orchard, S. On surface levelling in viscous liquids and gels. *Applied Scientific Research, Section A* **1963**, *11*, 451–464.

40. Saucy, D., International Coatings Exposition Conference, 2004.

41. Pearson, J. The instability of uniform viscous flow under rollers and spreaders. *Journal of Fluid Mechanics* **1960**, *7*, 481–500.

42. Wu, S. Rheology of high solid coatings. II. Analysis of combined sagging and leveling. *Journal of Applied Polymer Science* **1978**, *22*, 2783–2791.

43. Beeferman, H.; Bergren, D. Practical applications of rheology in the paint industry. *J. Paint Technol* **1966**, *38*.

44. Jong, L. Poly (acrylic acid) grafted soy carbohydrate as thickener for waterborne paints. *Materials Today Communications* **2020**, *23*, 100882.

45. Lu, C. F. Latex paint rheology and performance properties. *Industrial & engineering chemistry product research and development* **1985**, *24*, 412–417.

46. Johansen, K. I. Correlation between traditional methods for characterisation of sag and levelling of paints and rheological measurements. *Materials Today Communications* **2004**, *12*, 191–193.

47. Sarkar, N.; Lalk, R. H. Rheological correlation with application properties of latex paints. *Journal of Paint Technology* **1974**, *46*, 29–34.

48. Molenaar, F.; Svanholm, T.; Toussaint, A. Rheological behaviour of latexes in-can and during film drying. *Progress in organic coatings* **1997**, *30*, 141–158.

49. Murphy, J. *Paint Research Association Internal Report*; Internal Report; Melton Mowbray, Leics: Paint Research Association, 1968.

50. Eres, M.; Schwartz, L.; Roy, R. Fingering phenomena for driven coating films. *Physics of Fluids* **2000**, *12*, 1278–1295.

51. Schwartz, L. Theoretical and numerical modeling of coating flow on simple and complex substrates including rheology, drying and Marangoni effects. *Advances in coating and drying of thin films* **1999**, 105–128.

52. Roy, R.; Roberts, A.; Simpson, M. A lubrication model of coating flows over a curved substrate in space. **2002**.

53. Schwartz, L. W.; Eley, R. R. A Mathematical Model for Three-dimensional Coating Flow with Thixotropy. *Structure* **1959**, *58*, 470–494.

54. Rhys, H. I., *Machine Learning with R, the tidyverse, and mlr*; Manning: 2020.

55. Dinkgreve, M.; Paredes, J.; Denn, M. M.; Bonn, D. On different ways of measuring "the" yield stress. *Journal of non-Newtonian fluid mechanics* **2016**, *238*, 233–241.

56. Glass, J. Dynamics of Roll Spatter and Tracking. III: Importance of Extensional Viscosities. **1978**.

57. Strivens, T. The shear thickening effect in concentrated dispersion systems. *Journal of Colloid and Interface Science* **1976**, *57*, 476–487.

58. Kuge, Y. Study on the Workability of Paints-Forces Exerted During Brushing and the Rheological Characteristics of Paints. *Journal of Coatings Technology* **1983**, *55*, 59–64.

59. Deka, A.; Dey, N. Rheological studies of two component high build epoxy and polyurethane based high performance coatings. *Journal of Coatings Technology and Research* **2013**, *10*, 305–315.

60. Van der Kooij, H. M.; Sprakel, J. Watching paint dry; more exciting than it seems. *Soft Matter* **2015**, *11*, 6353–6359.

61. Optimizing Rheology for Paint and Coating Applications, 2015.

APPENDICES

Appendix A

PAINT FORMULATIONS

A.1 825 Formulation

% NV	Lbs/Gal	20 PVC with TiO2 Material	Architectural Acrylic Paint Formula Lbs	Gal	Non-Volatile Lbs	Gal
		GRIND:				
			Formula		**Non-Volatile**	
% NV	**Lbs/Gal**	**Material**	**Lbs**	**Gal**	**Lbs**	**Gal**
0	8.33	Water	75.78	9.10	0.00	0.00
25	9.19	Tamol 731A	5.75	0.63	1.44	0.11
98	8.35	BYK 022	0.19	0.02	0.19	0.02
1.5	7.18	Kathon LX 1.5%	0.23	0.03	0.00	0.00
25	8.26	Acrysol RM-2020	4.00	0.48	1.00	0.12
25	8.26	Acrysol RM-825	0.60	0.07	0.15	0.02
100	33.33	Ti-Pure R-902	83.71	2.51	83.71	2.51
0	8.66	Propylene Glycol	3.61	0.42	0.00	0.00
70	8.91	Tergitol 15-S-40	4.00	0.45	2.80	0.31
Grind Total			177.87	13.71	89.29	3.10
Pigment Total			83.71	2.51	83.71	2.51
Grind (2000 rpm) to Hegman 7+						
LETDOWN:						
			Formula		**Non-Volatile**	
% NV	**Lbs/Gal**	**Material**	**Lbs**	**Gal**	**Lbs**	**Gal**
		Grind	177.87	13.71	89.29	3.10
0	8.33	Water	20.00	2.40	0.00	0.00
98	8.35	BYK 022	0.20	0.02	0.20	0.02
50	8.82	Rhoplex SG 30	176.44	20.01	88.22	9.42
25	8.26	Acrysol RM-825	0.50	0.06	0.13	0.02
0	8.33	Water	20.12	2.42	0.00	0.00
0	7.93	Texanol	4.87	0.61	0.00	0.00
TOTAL			400.00	39.23	177.83	12.56
Paint properties						
Weight per gallon	10.20					
Viscosity						
% NV by weight	44.46					
% NV by volume	32.01					
PVC	20.00					

A.2 2020 Formulation

% NV	Lbs/Gal	20 PVC with TiO Architectural Acrylic Paint				
GRIND:						
			Formula		**Non-Volatile**	
% NV	**Lbs/Gal**	**Material**	**Lbs**	**Gal**	**Lbs**	**Gal**
0	8.33	Water	64.08	7.69	0.00	0.00
25	9.19	Tamol 731A	5.75	0.63	1.44	0.11
98	8.35	BYK 022	0.19	0.02	0.19	0.02
1.5	7.18	Kathon LX 1.5%	0.23	0.03	0.00	0.00
25	8.26	Acrysol RM-2020	15.00	1.82	3.75	0.46
100	33.33	Ti-Pure R-902	83.71	2.51	83.71	2.51
0	8.66	Propylene Glycol	3.61	0.42	0.00	0.00
70	8.91	Tergitol 15-S-40	4.00	0.45	2.80	0.31
Grind Total			176.57	13.57	91.89	3.43
Pigment Total			83.71	2.51	83.71	2.51
Grind (2000 rpm) to Hegman 7+						
LETDOWN:						
			Formula		**Non-Volatile**	
% NV	**Lbs/Gal**	**Material**	**Lbs**	**Gal**	**Lbs**	**Gal**
		Grind	176.57	13.57	91.89	3.43
0	8.33	Water	0.00	0.00	0.00	0.00
98	8.35	BYK 022	0.20	0.02	0.20	0.02
50	8.82	Rhoplex SG 30	176.44	20.01	88.22	9.42
25	8.26	Acrysol RM-2020	15.51	1.88	3.88	0.48
0	8.33	Water	25.50	3.06	0.00	0.00
0	7.93	Texanol	4.87	0.61	0.00	0.00
TOTAL			399.09	39.15	184.18	13.35
Paint properties						
Weight per gallon	10.19					
Viscosity						
% NV by weight	46.15					
% NV by volume	34.09					
PVC	18.82					

A.3 100% HEC Formulation

% NV	Lbs/Gal	Material	20 PVC with TiO2 — Formula — Lbs	Gal	Non-Volatile — Lbs	Gal
			Architectural Acrylic Paint			
GRIND:						
			Formula		**Non-Volatile**	
% NV	**Lbs/Gal**	**Material**	**Lbs**	**Gal**	**Lbs**	**Gal**
0	8.33	Water	55.08	6.61	0.00	0.00
25	9.19	Tamol 731A	5.75	0.63	1.44	0.11
98	8.35	BYK 022	0.19	0.02	0.19	0.02
1.5	7.18	Kathon LX 1.5%	0.23	0.03	0.00	0.00
25	8.26	Acrysol RM-2020	4.00	0.48	1.00	0.12
2	8.32	2% Natrosol 250 HI	20.00	2.41	0.40	0.05
100	33.33	Ti-Pure R-902	83.71	2.51	83.71	2.51
0	8.66	Propylene Glycol	3.61	0.42	0.00	0.00
70	8.91	Tergitol 15-S-40	4.00	0.45	2.80	0.31
Grind Total			176.57	13.56	89.54	3.14
Pigment Total			83.71	2.51	83.71	2.51
Grind (2000 rpm) to Hegman 7+						
LETDOWN:						
			Formula		**Non-Volatile**	
% NV	**Lbs/Gal**	**Material**	**Lbs**	**Gal**	**Lbs**	**Gal**
		Grind	176.57	13.56	89.54	3.14
0	8.33	Water	0.00	0.00	0.00	0.00
98	8.35	BYK 022	0.20	0.02	0.20	0.02
50	8.82	Rhoplex SG 30	176.44	20.01	88.22	9.42
2	8.32	2% Natrosol 250 HI	41.92	5.04	0.84	0.11
0	8.33	Water	0.00	0.00	0.00	0.00
0	7.93	Texanol	4.87	0.61	0.00	0.00
TOTAL			400.00	39.25	178.79	12.69

Paint properties	
Weight per gallon	10.19
Viscosity	
% NV by weight	44.70
% NV by volume	32.32
PVC	19.80

A.4 90% HEC Formulation

		20 PVC with TiO2	Architectural Acrylic Paint			
GRIND:						
			Formula		**Non-Volatile**	
% NV	**Lbs/Gal**	**Material**	**Lbs**	**Gal**	**Lbs**	**Gal**
0	8.33	Water	55.08	6.61	0.00	0.00
25	9.19	Tamol 731A	5.75	0.63	1.44	0.11
98	8.35	BYK 022	0.19	0.02	0.19	0.02
1.5	7.18	Kathon LX 1.5%	0.23	0.03	0.00	0.00
25	8.26	Acrysol RM-2020	4.00	0.48	1.00	0.12
2	8.32	2% Natrosol 250 HR	18.00	2.16	0.36	0.05
100	33.33	Ti-Pure R-902	83.71	2.51	83.71	2.51
0	8.66	Propylene Glycol	3.61	0.42	0.00	0.00
70	8.91	Tergitol 15-S-40	4.00	0.45	2.80	0.31
Grind Total			174.57	13.32	89.50	3.13
Pigment Total			83.71	2.51	83.71	2.51
Grind (2000 rpm) to Hegman 7+						
LETDOWN:						
			Formula		**Non-Volatile**	
% NV	**Lbs/Gal**	**Material**	**Lbs**	**Gal**	**Lbs**	**Gal**
		Grind	174.57	13.32	89.50	3.13
0	8.33	Water	6.19	0.74	0.00	0.00
98	8.35	BYK 022	0.20	0.02	0.20	0.02
50	8.82	Rhoplex SG 30	176.44	20.01	88.22	9.42
2	8.32	2% Natrosol 250 HR	37.73	4.54	0.75	0.10
0	8.33	Water	0.00	0.00	0.00	0.00
0	7.93	Texanol	4.87	0.61	0.00	0.00
TOTAL			400.00	39.24	178.67	12.67
Paint properties						
Weight per gallon		10.19				
Viscosity						
% NV by weight		44.67				
% NV by volume		32.28				
PVC		19.82				

A.5 80% HEC Formulation

% NV	Lbs/Gal	Material	20 PVC with TiO2	Architectural Acrylic Paint		
GRIND:						
			Formula		**Non-Volatile**	
% NV	**Lbs/Gal**	**Material**	**Lbs**	**Gal**	**Lbs**	**Gal**
0	8.33	Water	55.08	6.61	0.00	0.00
25	9.19	Tamol 731A	5.75	0.63	1.44	0.11
98	8.35	BYK 022	0.19	0.02	0.19	0.02
1.5	7.18	Kathon LX 1.5%	0.23	0.03	0.00	0.00
25	8.26	Acrysol RM-2020	4.00	0.48	1.00	0.12
2	8.32	2% Natrosol 250 HR	16.00	1.92	0.32	0.04
100	33.33	Ti-Pure R-902	83.71	2.51	83.71	2.51
0	8.66	Propylene Glycol	3.61	0.42	0.00	0.00
70	8.91	Tergitol 15-S-40	4.00	0.45	2.80	0.31
Grind Total			172.57	13.08	89.46	3.13
Pigment Total			83.71	2.51	83.71	2.51
Grind (2000 rpm) to Hegman 7+						
LETDOWN:						
			Formula		**Non-Volatile**	
% NV	**Lbs/Gal**	**Material**	**Lbs**	**Gal**	**Lbs**	**Gal**
		Grind	172.57	13.08	89.46	3.13
0	8.33	Water	12.38	1.49	0.00	0.00
98	8.35	BYK 022	0.20	0.02	0.20	0.02
50	8.82	Rhoplex SG 30	176.44	20.01	88.22	9.42
2	8.32	2% Natrosol 250 HR	33.54	4.03	0.67	0.09
0	8.33	Water	0.00	0.00	0.00	0.00
0	7.93	Texanol	4.87	0.61	0.00	0.00
TOTAL			400.00	39.24	178.54	12.65
Paint properties						
Weight per gallon		10.19				
Viscosity						
% NV by weight		44.64				
% NV by volume		32.24				
PVC		19.85				

A.6 70% HEC Formulation

% NV	Lbs/Gal	20 PVC with TiO2 Material	Architectural Acrylic Paint Formula Lbs	Gal	Non-Volatile Lbs	Gal
GRIND:						
			Formula		**Non-Volatile**	
% NV	**Lbs/Gal**	**Material**	**Lbs**	**Gal**	**Lbs**	**Gal**
0	8.33	Water	55.08	6.61	0.00	0.00
25	9.19	Tamol 731A	5.75	0.63	1.44	0.11
98	8.35	BYK 022	0.19	0.02	0.19	0.02
1.5	7.18	Kathon LX 1.5%	0.23	0.03	0.00	0.00
25	8.26	Acrysol RM-2020	4.00	0.48	1.00	0.12
2	8.32	2% Natrosol 250 HR	14.00	1.68	0.28	0.04
100	33.33	Ti-Pure R-902	83.71	2.51	83.71	2.51
0	8.66	Propylene Glycol	3.61	0.42	0.00	0.00
70	8.91	Tergitol 15-S-40	4.00	0.45	2.80	0.31
Grind Total			170.57	12.84	89.42	3.12
Pigment Total			83.71	2.51	83.71	2.51
Grind (2000 rpm) to Hegman 7+						
LETDOWN:						
			Formula		**Non-Volatile**	
% NV	**Lbs/Gal**	**Material**	**Lbs**	**Gal**	**Lbs**	**Gal**
		Grind	170.57	12.84	89.42	3.12
0	8.33	Water	18.58	2.23	0.00	0.00
98	8.35	BYK 022	0.20	0.02	0.20	0.02
50	8.82	Rhoplex SG 30	176.44	20.01	88.22	9.42
2	8.32	2% Natrosol 250 HR	29.34	3.53	0.59	0.08
0	8.33	Water	0.00	0.00	0.00	0.00
0	7.93	Texanol	4.87	0.61	0.00	0.00
TOTAL			400.00	39.24	178.42	12.64
Paint properties						
Weight per gallon		10.19				
Viscosity						
% NV by weight		44.60				
% NV by volume		32.20				
PVC		19.87				

A.7   60% HEC Formulation

% NV	Lbs/Gal	20 PVC with TiO2 — Material	Architectural Acrylic Paint — Formula Lbs	Gal	Non-Volatile Lbs	Gal
GRIND:						
			Formula		**Non-Volatile**	
% NV	**Lbs/Gal**	**Material**	**Lbs**	**Gal**	**Lbs**	**Gal**
0	8.33	Water	55.08	6.61	0.00	0.00
25	9.19	Tamol 731A	5.75	0.63	1.44	0.11
98	8.35	BYK 022	0.19	0.02	0.19	0.02
1.5	7.18	Kathon LX 1.5%	0.23	0.03	0.00	0.00
25	8.26	Acrysol RM-2020	4.00	0.48	1.00	0.12
2	8.32	2% Natrosol 250 HR	12.00	1.44	0.24	0.03
100	33.33	Ti-Pure R-902	83.71	2.51	83.71	2.51
0	8.66	Propylene Glycol	3.61	0.42	0.00	0.00
70	8.91	Tergitol 15-S-40	4.00	0.45	2.80	0.31
Grind Total			168.57	12.60	89.38	3.12
Pigment Total			83.71	2.51	83.71	2.51
Grind (2000 rpm) to Hegman 7+						
LETDOWN:						
			Formula		**Non-Volatile**	
% NV	**Lbs/Gal**	**Material**	**Lbs**	**Gal**	**Lbs**	**Gal**
		Grind	168.57	12.60	89.38	3.12
0	8.33	Water	24.77	2.97	0.00	0.00
98	8.35	BYK 022	0.20	0.02	0.20	0.02
50	8.82	Rhoplex SG 30	176.44	20.01	88.22	9.42
2	8.32	2% Natrosol 250 HR	25.15	3.02	0.50	0.07
0	8.33	Water	0.00	0.00	0.00	0.00
0	7.93	Texanol	4.87	0.61	0.00	0.00
TOTAL			400.00	39.24	178.30	12.62
Paint properties						
Weight per gallon		10.19				
Viscosity						
% NV by weight		44.57				
% NV by volume		32.16				
PVC		19.90				

A.8 50% HEC Formulation

		20 PVC with TiO2	Architectural Acrylic Paint			
GRIND:						
			Formula		**Non-Volatile**	
% NV	**Lbs/Gal**	**Material**	**Lbs**	**Gal**	**Lbs**	**Gal**
0	8.33	Water	55.08	6.61	0.00	0.00
25	9.19	Tamol 731A	5.75	0.63	1.44	0.11
98	8.35	BYK 022	0.19	0.02	0.19	0.02
1.5	7.18	Kathon LX 1.5%	0.23	0.03	0.00	0.00
25	8.26	Acrysol RM-2020	4.00	0.48	1.00	0.12
2	8.32	2% Natrosol 250 HR	10.00	1.20	0.20	0.03
100	33.33	Ti-Pure R-902	83.71	2.51	83.71	2.51
0	8.66	Propylene Glycol	3.61	0.42	0.00	0.00
70	8.91	Tergitol 15-S-40	4.00	0.45	2.80	0.31
Grind Total			166.57	12.36	89.34	3.11
Pigment Total			83.71	2.51	83.71	2.51
Grind (2000 rpm) to Hegman 7+						
LETDOWN:						
			Formula		**Non-Volatile**	
% NV	**Lbs/Gal**	**Material**	**Lbs**	**Gal**	**Lbs**	**Gal**
		Grind	166.57	12.36	89.34	3.11
0	8.33	Water	30.96	3.72	0.00	0.00
98	8.35	BYK 022	0.20	0.02	0.20	0.02
50	8.82	Rhoplex SG 30	176.44	20.01	88.22	9.42
2	8.32	2% Natrosol 250 HR	20.96	2.52	0.42	0.05
0	8.33	Water	0.00	0.00	0.00	0.00
0	7.93	Texanol	4.87	0.61	0.00	0.00
TOTAL			400.00	39.24	178.17	12.61
Paint properties						
Weight per gallon		10.19				
Viscosity						
% NV by weight		44.54				
% NV by volume		32.12				
PVC		19.92				

A.9 40% HEC Formulation

% NV	Lbs/Gal	Material	Lbs	Gal	Lbs	Gal
		20 PVC with TiO2	**Architectural Acrylic Paint**			
GRIND:						
			Formula		**Non-Volatile**	
% NV	**Lbs/Gal**	**Material**	**Lbs**	**Gal**	**Lbs**	**Gal**
0	8.33	Water	55.08	6.61	0.00	0.00
25	9.19	Tamol 731A	5.75	0.63	1.44	0.11
98	8.35	BYK 022	0.19	0.02	0.19	0.02
1.5	7.18	Kathon LX 1.5%	0.23	0.03	0.00	0.00
25	8.26	Acrysol RM-2020	4.00	0.48	1.00	0.12
2	8.32	2% Natrosol 250 HR	8.00	0.96	0.16	0.02
100	33.33	Ti-Pure R-902	83.71	2.51	83.71	2.51
0	8.66	Propylene Glycol	3.61	0.42	0.00	0.00
70	8.91	Tergitol 15-S-40	4.00	0.45	2.80	0.31
Grind Total			164.57	12.12	89.30	3.11
Pigment Total			83.71	2.51	83.71	2.51
Grind (2000 rpm) to Hegman 7+						
LETDOWN:						
			Formula		**Non-Volatile**	
% NV	**Lbs/Gal**	**Material**	**Lbs**	**Gal**	**Lbs**	**Gal**
		Grind	164.57	12.12	89.30	3.11
0	8.33	Water	37.15	4.46	0.00	0.00
98	8.35	BYK 022	0.20	0.02	0.20	0.02
50	8.82	Rhoplex SG 30	176.44	20.01	88.22	9.42
2	8.32	2% Natrosol 250 HR	16.77	2.02	0.34	0.04
0	8.33	Water	0.00	0.00	0.00	0.00
0	7.93	Texanol	4.87	0.61	0.00	0.00
TOTAL			400.00	39.24	178.05	12.59
Paint properties						
Weight per gallon		10.19				
Viscosity						
% NV by weight		44.51				
% NV by volume		32.08				
PVC		19.95				

A.10 30% HEC Formulation

% NV	Lbs/Gal	20 PVC with TiO2 Material	Architectural Acrylic Paint Formula Lbs	Gal	Non-Volatile Lbs	Gal
GRIND:						
			Formula		**Non-Volatile**	
% NV	**Lbs/Gal**	**Material**	**Lbs**	**Gal**	**Lbs**	**Gal**
0	8.33	Water	55.08	6.61	0.00	0.00
25	9.19	Tamol 731A	5.75	0.63	1.44	0.11
98	8.35	BYK 022	0.19	0.02	0.19	0.02
1.5	7.18	Kathon LX 1.5%	0.23	0.03	0.00	0.00
25	8.26	Acrysol RM-2020	4.00	0.48	1.00	0.12
2	8.32	2% Natrosol 250 HR	6.00	0.72	0.12	0.02
100	33.33	Ti-Pure R-902	83.71	2.51	83.71	2.51
0	8.66	Propylene Glycol	3.61	0.42	0.00	0.00
70	8.91	Tergitol 15-S-40	4.00	0.45	2.80	0.31
Grind Total			162.57	11.88	89.26	3.10
Pigment Total			83.71	2.51	83.71	2.51
Grind (2000 rpm) to Hegman 7+						
LETDOWN:						
			Formula		**Non-Volatile**	
% NV	**Lbs/Gal**	**Material**	**Lbs**	**Gal**	**Lbs**	**Gal**
		Grind	162.57	11.88	89.26	3.10
0	8.33	Water	43.35	5.20	0.00	0.00
98	8.35	BYK 022	0.20	0.02	0.20	0.02
50	8.82	Rhoplex SG 30	176.44	20.01	88.22	9.42
2	8.32	2% Natrosol 250 HR	12.57	1.51	0.25	0.03
0	8.33	Water	0.00	0.00	0.00	0.00
0	7.93	Texanol	4.87	0.61	0.00	0.00
TOTAL			400.00	39.24	177.92	12.57
Paint properties						
Weight per gallon		10.19				
Viscosity						
% NV by weight		44.48				
% NV by volume		32.04				
PVC		19.97				

A.11 20% HEC Formulation

% NV	Lbs/Gal	Material	Formula Lbs	Formula Gal	Non-Volatile Lbs	Non-Volatile Gal
		20 PVC with TiO2	**Architectural Acrylic Paint**			
GRIND:						
			Formula		**Non-Volatile**	
% NV	**Lbs/Gal**	**Material**	**Lbs**	**Gal**	**Lbs**	**Gal**
0	8.33	Water	55.08	6.61	0.00	0.00
25	9.19	Tamol 731A	5.75	0.63	1.44	0.11
98	8.35	BYK 022	0.19	0.02	0.19	0.02
1.5	7.18	Kathon LX 1.5%	0.23	0.03	0.00	0.00
25	8.26	Acrysol RM-2020	4.00	0.48	1.00	0.12
2	8.32	2% Natrosol 250 HR	4.00	0.48	0.08	0.01
100	33.33	Ti-Pure R-902	83.71	2.51	83.71	2.51
0	8.66	Propylene Glycol	3.61	0.42	0.00	0.00
70	8.91	Tergitol 15-S-40	4.00	0.45	2.80	0.31
Grind Total			**160.57**	**11.64**	**89.22**	**3.10**
Pigment Total			**83.71**	**2.51**	**83.71**	**2.51**
Grind (2000 rpm) to Hegman 7+						
LETDOWN:						
			Formula		**Non-Volatile**	
% NV	**Lbs/Gal**	**Material**	**Lbs**	**Gal**	**Lbs**	**Gal**
		Grind	160.57	11.64	89.22	3.10
0	8.33	Water	49.54	5.95	0.00	0.00
98	8.35	BYK 022	0.20	0.02	0.20	0.02
50	8.82	Rhoplex SG 30	176.44	20.01	88.22	9.42
2	8.32	2% Natrosol 250 HR	8.38	1.01	0.17	0.02
0	8.33	Water	0.00	0.00	0.00	0.00
0	7.93	Texanol	4.87	0.61	0.00	0.00
TOTAL			**400.00**	**39.24**	**177.80**	**12.56**
Paint properties						
Weight per gallon		10.19				
Viscosity						
% NV by weight		44.45				
% NV by volume		32.00				
PVC		20.00				

A.12 10% HEC Formulation

% NV	Lbs/Gal	20 PVC with TiO2 — Material	Architectural Acrylic Paint — Formula Lbs	Gal	Non-Volatile Lbs	Gal
GRIND:						
			Formula		**Non-Volatile**	
% NV	**Lbs/Gal**	**Material**	**Lbs**	**Gal**	**Lbs**	**Gal**
0	8.33	Water	55.08	6.61	0.00	0.00
25	9.19	Tamol 731A	5.75	0.63	1.44	0.11
98	8.35	BYK 022	0.19	0.02	0.19	0.02
1.5	7.18	Kathon LX 1.5%	0.23	0.03	0.00	0.00
25	8.26	Acrysol RM-2020	4.00	0.48	1.00	0.12
2	8.32	2% Natrosol 250 HR	2.00	0.24	0.04	0.01
100	33.33	Ti-Pure R-902	83.71	2.51	83.71	2.51
0	8.66	Propylene Glycol	3.61	0.42	0.00	0.00
70	8.91	Tergitol 15-S-40	4.00	0.45	2.80	0.31
Grind Total			158.57	11.39	89.18	3.09
Pigment Total			83.71	2.51	83.71	2.51
Grind (2000 rpm) to Hegman 7+						
LETDOWN:						
			Formula		**Non-Volatile**	
% NV	**Lbs/Gal**	**Material**	**Lbs**	**Gal**	**Lbs**	**Gal**
		Grind	158.57	11.39	89.18	3.09
0	8.33	Water	55.73	6.69	0.00	0.00
98	8.35	BYK 022	0.20	0.02	0.20	0.02
50	8.82	Rhoplex SG 30	176.44	20.01	88.22	9.42
2	8.32	2% Natrosol 250 HR	4.19	0.50	0.08	0.01
0	8.33	Water	0.00	0.00	0.00	0.00
0	7.93	Texanol	4.87	0.61	0.00	0.00
TOTAL			400.00	39.23	177.68	12.54
Paint properties						
Weight per gallon		10.20				
Viscosity						
% NV by weight		44.42				
% NV by volume		31.96				
PVC		20.03				

A.13 100% XG Formulation

% NV	Lbs/Gal	Material	Lbs	Gal	Lbs	Gal
		20 PVC with TiO	**Architectural Acrylic Paint**			
GRIND:						
			Formula		**Non-Volatile**	
% NV	**Lbs/Gal**	**Material**	**Lbs**	**Gal**	**Lbs**	**Gal**
0	8.33	Water	52.88	6.35	0.00	0.00
25	9.19	Tamol 731A	5.75	0.63	1.44	0.11
98	8.35	BYK 022	0.19	0.02	0.19	0.02
1.5	7.18	Kathon LX 1.5%	0.23	0.03	0.00	0.00
25	8.26	Acrysol RM-2020	4.00	0.48	1.00	0.12
2	7.99	2% Xanthan Gum	20.00	2.50	0.40	0.15
100	33.33	Ti-Pure R-902	83.71	2.51	83.71	2.51
0	8.66	Propylene Glycol	3.61	0.42	0.00	0.00
70	8.91	Tergitol 15-S-40	4.00	0.45	2.80	0.31
Grind Total			174.37	13.39	89.54	3.24
Pigment Total			83.71	2.51	83.71	2.51
Grind (2000 rpm) to Hegman 7+						
LETDOWN:						
			Formula		**Non-Volatile**	
% NV	**Lbs/Gal**	**Material**	**Lbs**	**Gal**	**Lbs**	**Gal**
		Grind	174.37	13.39	89.54	3.24
0	8.33	Water	0.00	0.00	0.00	0.00
98	8.35	BYK 022	0.20	0.02	0.20	0.02
50	8.82	Rhoplex SG 30	176.44	20.01	88.22	9.42
2	7.99	2% Xanthan Gum	44.12	5.52	0.88	0.33
0	8.33	Water	0.00	0.00	0.00	0.00
0	7.93	Texanol	4.87	0.61	0.00	0.00
TOTAL			400.00	39.56	178.84	13.01
Paint properties						
Weight per gallon	10.11					
Viscosity						
% NV by weight	44.71					
% NV by volume	32.88					
PVC	19.30					

A.14 90% XG Formulation

% NV	Lbs/Gal	Material	Formula Lbs	Formula Gal	Non-Volatile Lbs	Non-Volatile Gal
		20 PVC with TiO2	Architectural Acrylic Paint			
GRIND:						
			Formula		**Non-Volatile**	
% NV	**Lbs/Gal**	**Material**	**Lbs**	**Gal**	**Lbs**	**Gal**
0	8.33	Water	52.88	6.35	0.00	0.00
25	9.19	Tamol 731A	5.75	0.63	1.44	0.11
98	8.35	BYK 022	0.19	0.02	0.19	0.02
1.5	7.18	Kathon LX 1.5%	0.23	0.03	0.00	0.00
25	8.26	Acrysol RM-2020	4.00	0.48	1.00	0.12
2	7.99	2% Xanthan Gum	18.00	2.25	0.36	0.14
100	33.33	Ti-Pure R-902	83.71	2.51	83.71	2.51
0	8.66	Propylene Glycol	3.61	0.42	0.00	0.00
70	8.91	Tergitol 15-S-40	4.00	0.45	2.80	0.31
Grind Total			172.37	13.14	89.50	3.22
Pigment Total			83.71	2.51	83.71	2.51
Grind (2000 rpm) to Hegman 7+						
LETDOWN:						
			Formula		**Non-Volatile**	
% NV	**Lbs/Gal**	**Material**	**Lbs**	**Gal**	**Lbs**	**Gal**
		Grind	172.37	13.14	89.50	3.22
0	8.33	Water	6.41	0.77	0.00	0.00
98	8.35	BYK 022	0.20	0.02	0.20	0.02
50	8.82	Rhoplex SG 30	176.44	20.01	88.22	9.42
2	7.99	2% Xanthan Gum	39.71	4.97	0.79	0.30
0	8.33	Water	0.00	0.00	0.00	0.00
0	7.93	Texanol	4.87	0.61	0.00	0.00
TOTAL			400.00	39.53	178.71	12.96

Paint properties	
Weight per gallon	10.12
Viscosity	
% NV by weight	44.68
% NV by volume	32.79
PVC	19.38

A.15　80% XG Formulation

% NV	Lbs/Gal	Material	20 PVC with TiO2	Architectural Acrylic Paint		
GRIND:						
			Formula		**Non-Volatile**	
% NV	**Lbs/Gal**	**Material**	**Lbs**	**Gal**	**Lbs**	**Gal**
0	8.33	Water	52.88	6.35	0.00	0.00
25	9.19	Tamol 731A	5.75	0.63	1.44	0.11
98	8.35	BYK 022	0.19	0.02	0.19	0.02
1.5	7.18	Kathon LX 1.5%	0.23	0.03	0.00	0.00
25	8.26	Acrysol RM-2020	4.00	0.48	1.00	0.12
2	7.99	2% Xanthan Gum	16.00	2.00	0.32	0.12
100	33.33	Ti-Pure R-902	83.71	2.51	83.71	2.51
0	8.66	Propylene Glycol	3.61	0.42	0.00	0.00
70	8.91	Tergitol 15-S-40	4.00	0.45	2.80	0.31
Grind Total			**170.37**	**12.89**	**89.46**	**3.21**
Pigment Total			**83.71**	**2.51**	**83.71**	**2.51**
Grind (2000 rpm) to Hegman 7+						
LETDOWN:						
			Formula		**Non-Volatile**	
% NV	**Lbs/Gal**	**Material**	**Lbs**	**Gal**	**Lbs**	**Gal**
		Grind	170.37	12.89	89.46	3.21
0	8.33	Water	12.82	1.54	0.00	0.00
98	8.35	BYK 022	0.20	0.02	0.20	0.02
50	8.82	Rhoplex SG 30	176.44	20.01	88.22	9.42
2	7.99	2% Xanthan Gum	35.30	4.42	0.71	0.27
0	8.33	Water	0.00	0.00	0.00	0.00
0	7.93	Texanol	4.87	0.61	0.00	0.00
TOTAL			**400.00**	**39.50**	**178.58**	**12.91**
Paint properties						
Weight per gallon		10.13				
Viscosity						
% NV by weight		44.64				
% NV by volume		32.69				
PVC		19.45				

A.16 70% XG Formulation

% NV	Lbs/Gal	Material	Formula Lbs	Formula Gal	Non-Volatile Lbs	Non-Volatile Gal
		20 PVC with TiO2	**Architectural Acrylic Paint**			
GRIND:						
			Formula		**Non-Volatile**	
% NV	**Lbs/Gal**	**Material**	**Lbs**	**Gal**	**Lbs**	**Gal**
0	8.33	Water	52.88	6.35	0.00	0.00
25	9.19	Tamol 731A	5.75	0.63	1.44	0.11
98	8.35	BYK 022	0.19	0.02	0.19	0.02
1.5	7.18	Kathon LX 1.5%	0.23	0.03	0.00	0.00
25	8.26	Acrysol RM-2020	4.00	0.48	1.00	0.12
2	7.99	2% Xanthan Gum	14.00	1.75	0.28	0.11
100	33.33	Ti-Pure R-902	83.71	2.51	83.71	2.51
0	8.66	Propylene Glycol	3.61	0.42	0.00	0.00
70	8.91	Tergitol 15-S-40	4.00	0.45	2.80	0.31
Grind Total			168.37	12.64	89.42	3.19
Pigment Total			83.71	2.51	83.71	2.51
Grind (2000 rpm) to Hegman 7+						
LETDOWN:						
			Formula		**Non-Volatile**	
% NV	**Lbs/Gal**	**Material**	**Lbs**	**Gal**	**Lbs**	**Gal**
		Grind	168.37	12.64	89.42	3.19
0	8.33	Water	19.24	2.31	0.00	0.00
98	8.35	BYK 022	0.20	0.02	0.20	0.02
50	8.82	Rhoplex SG 30	176.44	20.01	88.22	9.42
2	7.99	2% Xanthan Gum	30.88	3.87	0.62	0.23
0	8.33	Water	0.00	0.00	0.00	0.00
0	7.93	Texanol	4.87	0.61	0.00	0.00
TOTAL			400.00	39.46	178.45	12.86
Paint properties						
Weight per gallon		10.14				
Viscosity						
% NV by weight		44.61				
% NV by volume		32.60				
PVC		19.52				

A.17 60% XG Formulation

% NV	Lbs/Gal	20 PVC with TiO2 Material	Architectural Acrylic Paint Formula Lbs	Gal	Non-Volatile Lbs	Gal
GRIND:						
			Formula		**Non-Volatile**	
% NV	**Lbs/Gal**	**Material**	**Lbs**	**Gal**	**Lbs**	**Gal**
0	8.33	Water	52.88	6.35	0.00	0.00
25	9.19	Tamol 731A	5.75	0.63	1.44	0.11
98	8.35	BYK 022	0.19	0.02	0.19	0.02
1.5	7.18	Kathon LX 1.5%	0.23	0.03	0.00	0.00
25	8.26	Acrysol RM-2020	4.00	0.48	1.00	0.12
2	7.99	2% Xanthan Gum	12.00	1.50	0.24	0.09
100	33.33	Ti-Pure R-902	83.71	2.51	83.71	2.51
0	8.66	Propylene Glycol	3.61	0.42	0.00	0.00
70	8.91	Tergitol 15-S-40	4.00	0.45	2.80	0.31
Grind Total			**166.37**	**12.39**	**89.38**	**3.18**
Pigment Total			**83.71**	**2.51**	**83.71**	**2.51**
Grind (2000 rpm) to Hegman 7+						
LETDOWN:						
			Formula		**Non-Volatile**	
% NV	**Lbs/Gal**	**Material**	**Lbs**	**Gal**	**Lbs**	**Gal**
		Grind	166.37	12.39	89.38	3.18
0	8.33	Water	25.65	3.08	0.00	0.00
98	8.35	BYK 022	0.20	0.02	0.20	0.02
50	8.82	Rhoplex SG 30	176.44	20.01	88.22	9.42
2	7.99	2% Xanthan Gum	26.47	3.31	0.53	0.20
0	8.33	Water	0.00	0.00	0.00	0.00
0	7.93	Texanol	4.87	0.61	0.00	0.00
TOTAL			**400.00**	**39.43**	**178.32**	**12.82**
Paint properties						
Weight per gallon		10.14				
Viscosity						
% NV by weight		44.58				
% NV by volume		32.50				
PVC		19.60				

A.18 50% XG Formulation

% NV	Lbs/Gal	Material	Formula Lbs	Formula Gal	Non-Volatile Lbs	Non-Volatile Gal
		20 PVC with TiO2	**Architectural Acrylic Paint**			
GRIND:						
			Formula		**Non-Volatile**	
% NV	**Lbs/Gal**	**Material**	**Lbs**	**Gal**	**Lbs**	**Gal**
0	8.33	Water	52.88	6.35	0.00	0.00
25	9.19	Tamol 731A	5.75	0.63	1.44	0.11
98	8.35	BYK 022	0.19	0.02	0.19	0.02
1.5	7.18	Kathon LX 1.5%	0.23	0.03	0.00	0.00
25	8.26	Acrysol RM-2020	4.00	0.48	1.00	0.12
2	7.99	2% Xanthan Gum	10.00	1.25	0.20	0.08
100	33.33	Ti-Pure R-902	83.71	2.51	83.71	2.51
0	8.66	Propylene Glycol	3.61	0.42	0.00	0.00
70	8.91	Tergitol 15-S-40	4.00	0.45	2.80	0.31
Grind Total			164.37	12.14	89.34	3.16
Pigment Total			83.71	2.51	83.71	2.51
Grind (2000 rpm) to Hegman 7+						
LETDOWN:						
			Formula		**Non-Volatile**	
% NV	**Lbs/Gal**	**Material**	**Lbs**	**Gal**	**Lbs**	**Gal**
		Grind	164.37	12.14	89.34	3.16
0	8.33	Water	32.06	3.85	0.00	0.00
98	8.35	BYK 022	0.20	0.02	0.20	0.02
50	8.82	Rhoplex SG 30	176.44	20.01	88.22	9.42
2	7.99	2% Xanthan Gum	22.06	2.76	0.44	0.17
0	8.33	Water	0.00	0.00	0.00	0.00
0	7.93	Texanol	4.87	0.61	0.00	0.00
TOTAL			400.00	39.40	178.19	12.77
Paint properties						
Weight per gallon		10.15				
Viscosity						
% NV by weight		44.55				
% NV by volume		32.40				
PVC		19.67				

A.19 40% XG Formulation

% NV	Lbs/Gal	Material	20 PVC with TiO2	Architectural Acrylic Paint		
GRIND:						
			Formula		Non-Volatile	
% NV	**Lbs/Gal**	**Material**	**Lbs**	**Gal**	**Lbs**	**Gal**
0	8.33	Water	52.88	6.35	0.00	0.00
25	9.19	Tamol 731A	5.75	0.63	1.44	0.11
98	8.35	BYK 022	0.19	0.02	0.19	0.02
1.5	7.18	Kathon LX 1.5%	0.23	0.03	0.00	0.00
25	8.26	Acrysol RM-2020	4.00	0.48	1.00	0.12
2	7.99	2% Xanthan Gum	8.00	1.00	0.16	0.06
100	33.33	Ti-Pure R-902	83.71	2.51	83.71	2.51
0	8.66	Propylene Glycol	3.61	0.42	0.00	0.00
70	8.91	Tergitol 15-S-40	4.00	0.45	2.80	0.31
Grind Total			162.37	11.89	89.30	3.15
Pigment Total			83.71	2.51	83.71	2.51
Grind (2000 rpm) to Hegman 7+						
LETDOWN:						
			Formula		Non-Volatile	
% NV	**Lbs/Gal**	**Material**	**Lbs**	**Gal**	**Lbs**	**Gal**
		Grind	162.37	11.89	89.30	3.15
0	8.33	Water	38.47	4.62	0.00	0.00
98	8.35	BYK 022	0.20	0.02	0.20	0.02
50	8.82	Rhoplex SG 30	176.44	20.01	88.22	9.42
2	7.99	2% Xanthan Gum	17.65	2.21	0.35	0.13
0	8.33	Water	0.00	0.00	0.00	0.00
0	7.93	Texanol	4.87	0.61	0.00	0.00
TOTAL			400.00	39.36	178.07	12.72
Paint properties						
Weight per gallon		10.16				
Viscosity						
% NV by weight		44.52				
% NV by volume		32.31				
PVC		19.75				

A.20 30% XG Formulation

% NV	Lbs/Gal	Material	Formula Lbs	Formula Gal	Non-Volatile Lbs	Non-Volatile Gal
		20 PVC with TiO2 Architectural Acrylic Paint				
GRIND:						
			Formula		**Non-Volatile**	
% NV	**Lbs/Gal**	**Material**	**Lbs**	**Gal**	**Lbs**	**Gal**
0	8.33	Water	52.88	6.35	0.00	0.00
25	9.19	Tamol 731A	5.75	0.63	1.44	0.11
98	8.35	BYK 022	0.19	0.02	0.19	0.02
1.5	7.18	Kathon LX 1.5%	0.23	0.03	0.00	0.00
25	8.26	Acrysol RM-2020	4.00	0.48	1.00	0.12
2	7.99	2% Xanthan Gum	6.00	0.75	0.12	0.05
100	33.33	Ti-Pure R-902	83.71	2.51	83.71	2.51
0	8.66	Propylene Glycol	3.61	0.42	0.00	0.00
70	8.91	Tergitol 15-S-40	4.00	0.45	2.80	0.31
Grind Total			**160.37**	**11.64**	**89.26**	**3.13**
Pigment Total			**83.71**	**2.51**	**83.71**	**2.51**
Grind (2000 rpm) to Hegman 7+						
LETDOWN:						
			Formula		**Non-Volatile**	
% NV	**Lbs/Gal**	**Material**	**Lbs**	**Gal**	**Lbs**	**Gal**
		Grind	160.37	11.64	89.26	3.13
0	8.33	Water	44.88	5.39	0.00	0.00
98	8.35	BYK 022	0.20	0.02	0.20	0.02
50	8.82	Rhoplex SG 30	176.44	20.01	88.22	9.42
2	7.99	2% Xanthan Gum	13.24	1.66	0.26	0.10
0	8.33	Water	0.00	0.00	0.00	0.00
0	7.93	Texanol	4.87	0.61	0.00	0.00
TOTAL			**400.00**	**39.33**	**177.94**	**12.67**
Paint properties						
Weight per gallon		10.17				
Viscosity						
% NV by weight		44.48				
% NV by volume		32.21				
PVC		19.82				

A.21 20% XG Formulation

% NV	Lbs/Gal	20 PVC with TiO2 Material	Architectural Acrylic Paint Formula Lbs	Gal	Non-Volatile Lbs	Gal
GRIND:						
			Formula		**Non-Volatile**	
% NV	**Lbs/Gal**	**Material**	**Lbs**	**Gal**	**Lbs**	**Gal**
0	8.33	Water	52.88	6.35	0.00	0.00
25	9.19	Tamol 731A	5.75	0.63	1.44	0.11
98	8.35	BYK 022	0.19	0.02	0.19	0.02
1.5	7.18	Kathon LX 1.5%	0.23	0.03	0.00	0.00
25	8.26	Acrysol RM-2020	4.00	0.48	1.00	0.12
2	7.99	2% Xanthan Gum	4.00	0.50	0.08	0.03
100	33.33	Ti-Pure R-902	83.71	2.51	83.71	2.51
0	8.66	Propylene Glycol	3.61	0.42	0.00	0.00
70	8.91	Tergitol 15-S-40	4.00	0.45	2.80	0.31
Grind Total			158.37	11.39	89.22	3.11
Pigment Total			83.71	2.51	83.71	2.51
Grind (2000 rpm) to Hegman 7+						
LETDOWN:						
			Formula		**Non-Volatile**	
% NV	**Lbs/Gal**	**Material**	**Lbs**	**Gal**	**Lbs**	**Gal**
		Grind	158.37	11.39	89.22	3.11
0	8.33	Water	51.30	6.16	0.00	0.00
98	8.35	BYK 022	0.20	0.02	0.20	0.02
50	8.82	Rhoplex SG 30	176.44	20.01	88.22	9.42
2	7.99	2% Xanthan Gum	8.82	1.10	0.18	0.07
0	8.33	Water	0.00	0.00	0.00	0.00
0	7.93	Texanol	4.87	0.61	0.00	0.00
TOTAL			400.00	39.30	177.81	12.62
Paint properties						
Weight per gallon		10.18				
Viscosity						
% NV by weight		44.45				
% NV by volume		32.12				
PVC		19.90				

A.22 10% XG Formulation

		20 PVC with TiO2	Architectural Acrylic Paint			
GRIND:						
			Formula		**Non-Volatile**	
% NV	**Lbs/Gal**	**Material**	**Lbs**	**Gal**	**Lbs**	**Gal**
0	8.33	Water	52.88	6.35	0.00	0.00
25	9.19	Tamol 731A	5.75	0.63	1.44	0.11
98	8.35	BYK 022	0.19	0.02	0.19	0.02
1.5	7.18	Kathon LX 1.5%	0.23	0.03	0.00	0.00
25	8.26	Acrysol RM-2020	4.00	0.48	1.00	0.12
2	7.99	2% Xanthan Gum	2.00	0.25	0.04	0.02
100	33.33	Ti-Pure R-902	83.71	2.51	83.71	2.51
0	8.66	Propylene Glycol	3.61	0.42	0.00	0.00
70	8.91	Tergitol 15-S-40	4.00	0.45	2.80	0.31
Grind Total			156.37	11.14	89.18	3.10
Pigment Total			83.71	2.51	83.71	2.51
Grind (2000 rpm) to Hegman 7+						
LETDOWN:						
			Formula		**Non-Volatile**	
% NV	**Lbs/Gal**	**Material**	**Lbs**	**Gal**	**Lbs**	**Gal**
		Grind	156.37	11.14	89.18	3.10
0	8.33	Water	57.71	6.93	0.00	0.00
98	8.35	BYK 022	0.20	0.02	0.20	0.02
50	8.82	Rhoplex SG 30	176.44	20.01	88.22	9.42
2	7.99	2% Xanthan Gum	4.41	0.55	0.09	0.03
0	8.33	Water	0.00	0.00	0.00	0.00
0	7.93	Texanol	4.87	0.61	0.00	0.00
TOTAL			400.00	39.27	177.68	12.57
Paint properties						
Weight per gallon		10.19				
Viscosity						
% NV by weight		44.42				
% NV by volume		32.02				
PVC		19.97				

Appendix B

MACHINE LEARNING CODE

B.1 Generalized Additive Model Code

```
library(tidyverse)
library(mlr)
library(parallelMap)

formulationDataPostEN <- read.csv("PATH TO FORMULATION DATA")
formulationDataPostENTib <- as_tibble(formulationDataPostEN) %>%
select(c(-1))
formulationDataTibPostEN

formulationData <- read.csv("PATH TO FORMULATION DATA")
formulationDataTib <- as_tibble(formulationData) %>%
select(c(-"Leveling_Rating", -"Run_Number", -(1:4), -(7:26)))
formulationDataTib

gamTask <- makeRegrTask(data = formulationDataTib, target = "AntiSag_Index")
imputeMethod <- imputeLearner("regr.rpart")
gamLearner <- makeLearner("regr.gamboost")
gamImputeWrapper <- makeImputeWrapper("regr.gamboost",
classes = list(numeric = imputeMethod))
gamFeatSelControl <- makeFeatSelControlSequential(method = "sfbs")
kFold <- makeResampleDesc("CV", iters = 10)
gamFeatSelWrapper <- makeFeatSelWrapper(learner = gamImputeWrapper,
resampling = kFold,
control = gamFeatSelControl)
holdout <- makeResampleDesc("Holdout")
gamCV <- resample(gamFeatSelWrapper, gamTask, resampling = holdout)
gamCV

library(parallel)
library(parallelMap)
parallelStartSocket(cpus = 5)
gamModel <- train(gamLearner, gamTask)
parallelStop()
gamModelData <- getLearnerModel(gamModel)
```

```
par(mfrow = c(3, 3))
plot(gamModelData, type = "l")
plot(gamModelData$fitted(), resid(gamModelData))
qqnorm(resid(gamModelData))
qqline(resid(gamModelData))
par(mfrow = c(1, 1))

gamModelData
```

B.2   Elastic Net Code

```
library(tidyverse)
library(mlr)
library(parallelMap)

formulationData <- read.csv("PATH TO FORMULATION DATA")
formulationDataTib <- as_tibble(formulationData) %>%
select(c(-"Leveling_Rating", -"Run_Number", -(1:4), -(7:26)))
formulationDataTib
formulationDataTask <- makeRegrTask(data = formulationDataTib, target = "AntiSag_I

elastic <- makeLearner("regr.glmnet", id = "elastic")

elasticParamSpace <- makeParamSet(
makeNumericParam("s", lower = 0, upper = 70),
makeNumericParam("alpha", lower = 0, upper = 1))

randSearch <- makeTuneControlRandom(maxit = 400)

cvForTuning <- makeResampleDesc("RepCV", folds = 5, reps = 10)

parallelStartSocket(cpus = 5)

tunedElasticPars <- tuneParams(elastic, task = formulationDataTask,
resampling = cvForTuning,
par.set = elasticParamSpace,
control = randSearch)
parallelStop()

tunedElasticPars

elasticTuningData <- generateHyperParsEffectData(tunedElasticPars)
```

```
plotHyperParsEffect(elasticTuningData, x = "s", y = "alpha",
z = "mse.test.mean", interpolate = "regr.kknn",
plot.type = "heatmap") +
scale_fill_gradientn(colours = terrain.colors(5)) +
geom_point(x = tunedElasticPars$x$s, y = tunedElasticPars$x$alpha,
col = "white") +
theme_bw()

tunedElastic <- setHyperPars(elastic, par.vals = tunedElasticPars$x)
tunedElasticModel <- train(tunedElastic, formulationDataTask)

elasticModelData <- getLearnerModel(tunedElasticModel)
elasticCoefs <- coef(elasticModelData, s = tunedElasticPars$x$s)


coefTib <- tibble(Coef = rownames(elasticCoefs)[-1])

coefTib$Elastic <- as.vector(elasticCoefs)[-1]

coefUntidy <- gather(coefTib, key = Model, value = Beta, -Coef)
ggplot(coefUntidy, aes(reorder(Coef, Beta), Beta, fill = Model)) +
geom_bar(stat = "identity", position = "dodge", col = "black") +
facet_wrap(~ Model) +
theme_bw() +
theme(axis.text.x = element_text(angle = 90, hjust = 1, vjust = 0.5))
```